Research Article

Effect of the Noble Metals Addition on the Oxidation Behavior of Ni₃Al

J. J. Ramos-Hernandez [iD],[1] **J. Porcayo-Calderon** [iD],[2] **J. G. Gonzalez-Rodriguez**,[2] **Jan Mayén**,[3] **G. Lara-Rodriguez**,[4] **V. M. Salinas-Bravo** [iD],[5] **and L. Martinez-Gomez** [iD][6,7]

[1]*Facultad de Química, Universidad Nacional Autónoma de Mexico, Edificio B, Cd. Universitaria, 04510 Ciudad de Mexico, Mexico*
[2]*CIICAp, Universidad Autónoma del Estado de Morelos, Avenida Universidad 1001, 62209 Cuernavaca, MOR, Mexico*
[3]*CIATEQ A.C., Eje 126 No. 225, Zona Industrial, 78395 San Luis Potosí, SLP, Mexico*
[4]*Instituto de Investigaciones en Materiales, Universidad Nacional Autónoma de Mexico, Cd. Universitaria, 04510 Ciudad de Mexico, Mexico*
[5]*Instituto Nacional de Electricidad y Energías Limpias, Avenida Reforma 113, Colonia Palmira, 62490 Cuernavaca, MOR, Mexico*
[6]*Instituto de Ciencias Físicas, Universidad Nacional Autónoma de Mexico, Avenida Universidad s/n, 62210 Cuernavaca, MOR, Mexico*
[7]*Corrosion y Protección (CyP), Buffon 46, 11590 Mexico City, Mexico*

Correspondence should be addressed to J. Porcayo-Calderon; jporcayoc@gmail.com

Received 6 July 2017; Revised 12 October 2017; Accepted 1 November 2017; Published 17 January 2018

Academic Editor: Amit Bandyopadhyay

This paper discusses the effect of the addition of noble metals on the microstructure, mechanism, and oxidation kinetics of the Ni₃Al intermetallic alloy. Ni₃Al was doped with 1% (atomic percent) of Au, Ag, Pd, and Pt. Oxidation behavior of the alloys was evaluated at 900, 1000, and 1100°C in O_2 for 24 hours. XRD analysis showed that the addition of noble metals favored the oxide growth on preferential crystallographic planes. In addition, the preferential substitution of the noble metals in the Ni₃Al structure modifies the surface composition by increasing the Al/Ni ratio. It was observed that most of the alloys showed a subparabolic behavior, and only the intermetallic base and the alloy doped with Ag show a parabolic behavior at 900°C. The developed oxides were analyzed both superficially and in cross section by scanning electron microscopy (SEM) and energy dispersive X-ray analysis (EDXA). It was evident that only the intermetallic base showed the formation of a duplex oxide scale (Al_2O_3/NiO). The alloys doped with noble metals showed the oxide growth practically of pure Al_2O_3. This was due to a decrease in the diffusion of the Ni cations because of the presence of the noble metals in the crystalline structure.

1. Introduction

Ni₃Al intermetallic compounds are excellent candidates for high-temperature structural applications due to their thermochemical and mechanical properties. They can perform beyond conventional temperatures because of their excellent resistance to corrosion and oxidation [1]. During solidification of an alloy with stoichiometry close to that of Ni₃Al, there is in the liquid phase a competition for phase stability between β_{NiAl}, γ'_{Ni3Al}, and γ_{Ni} with stable eutectic (β-γ'), metastable (β-γ), and peritectic (γ'-γ) phases which have

common borders in the Ni-Al binary diagram. Because the region of phase stability γ' is very narrow, any deviation in the Ni/Al ratio favors the stability of any of the aforementioned phases; that is, an increase in the Ni content tends to favor the stability of γ'-γ phase. According to Verin [2], the microstructure of the Ni-23Al-0.001Ce-0.004Co (at %) is composed of a combination of dendritic phases γ' and γ, where the matrix is the phase γ' and the interdendritic phase is the phase γ; similar results were obtained by Chiba and Hanada [3] for the alloy Ni-23Al (at %) and Jozwik et al. [4] for the alloy Ni-22Al-0.002Zr-0.001B (at %). Moreover, Hunziker

and Kurz [5] mentioned that the directional solidification of intermetallic Ni-25Al (at %) shows a microstructure where the phases β, γ, and γ' are found. In this case, the γ' phase is formed during cooling of metastable eutectic β-γ. It has been shown that there are subsequent transformations after the solidification process, which complicates the interpretation of the phases produced.

On the other hand, the solidification rate is a factor that influences the microstructure of the alloy. When the solidification is slow, the convection in the liquid phase favors formation of a single γ'-phase. However, in a rapid solidification process, there is little convection in the liquid phase and it promotes the formation of a structure with phases γ'' and β [6]. The addition of a third element to the Ni-Al system may stabilize or destabilize a given phase. According to Inoue et al. [7], the addition of Cr, Mn, Fe, Co, or Si destabilizes the phase γ', and according to Goetzinger et al. [8], the addition of Ti stabilizes the phase. Sun et al. [9] indicate that Pd, Ag, and Cu are elements forming the γ phase, while Pint et al. [10] show that Pt promotes the reduction of the temperature of the phase transformation from β to γ' during the process of cooling and phase transformation from γ' to β during heating.

During the oxidation process, β and γ' phases play an important role due to their content of Al [11]. According to Haerig and Hofmann [12], in the early stages of the oxidation process, NiO and Al_2O_3 are formed simultaneously due to the diffusion of cations towards the outside of the alloy. Bardi et al. [13] show that the growth of the oxide is in the form of islands. Al consumption owing to the formation of Al_2O_3 diminishes the aluminum content below 17% (at %), which is the content needed to form the outer protective layer [14]. This favors the growth of NiO onto the Al_2O_3 layer. This pattern occurs because of the conducting properties of the formed oxides: Al_2O_3 is an amphoteric oxide (movement of cations and anions is possible) allowing outward diffusion of Ni^+ cations. Al_2O_3 forms internally due to inward diffusion of O^{2-} anions, while NiO is a p-type conductor, which preferably promotes conduction of cations [15–17]. Al_2O_3 growth onto alloys such as Ni_3Al can adopt different crystallographic arrangements: between 427 and 927°C, the γ-Al_2O_3 phase is stable; until 1077°C, the θ-Al_2O_3 phase is stable; and above 1077°C, the α-Al_2O_3 phase is stable [18]. The $\theta \rightarrow \alpha$ transformation is accompanied by a change in the transport properties of the scale. The θ-Al_2O_3 scale mainly grows by outward diffusion of cations, forming cavities in the scale/alloy interface, resulting in the deterioration of the adhesion layer on the substrate. In contrast, the growth of α scale is dependent on the diffusion of the O^{2-} anion inwards, so that the oxide fills the preformed cavities. This improves the adhesion of the layer on the substrate. Therefore, it is desirable for the growth of an α-Al_2O_3 layer [1, 14]. It has been observed that the only growth of an outer scale of Al_2O_3 is possible under the following conditions, by increasing both the temperature and concentration of Al [12], where the oxidation process is carried out at oxygen partial pressures below the equilibrium of NiO formation [13, 19–21] and also in alloys which were implanted with B^+ and Cr^+ ions [14]. Increasing the oxygen partial pressure and temperature, it is possible to form the spinel $NiAl_2O_4$ at the NiO/Al_2O_3 interface [22].

Garza et al. [23] attributed this behavior to the difference between the free energies of formation of Al_2O_3 and NiO which is four times larger than that between Al_2O_3 and $NiAl_2O_4$. Velon and Olefjord [15] mentioned that the spinel could also be formed in the initial stages of oxidation at low temperatures (300°C).

A key aspect to increase the oxidation resistance of an alloy is to improve the adherence of the protective oxide mainly because most applications implicate high-temperature thermal cycles [13, 24]. The most effective method is the addition of elements or compounds such as Hf, Y, Zr, Cr, Pd, Pt, and SiC [25–31], which can change the localized concentration of aluminum and reduce its growth rate. Gleeson et al. [32] indicate that the addition of Pt has beneficial effects in promoting the formation of a stable Al_2O_3 scale. Pt is an unreactive element whose addition decreases the chemical activity of Al in the γ' phase, and it increases the Al/Ni ratio, which promotes the formation of Al_2O_3 in certain crystallographic planes and increases the Al diffusion into the formed scale. It has been calculated that the preferential site of substitution of noble metals like Ag, Au, Pd, and Pt in the Ni_3Al structure occurs in locations where there are normally nickel atoms [33–37]; therefore, the addition of these elements can modify the oxidation behavior of the alloy. Therefore, this paper evaluates the effect of the addition of these elements in low concentration (1 at.%) on the oxidation behavior of the Ni_3Al intermetallic alloy.

2. Experimental Procedure

The intermetallic alloys with nominal composition $Ni_{75}Al_{25}$ and $Ni_{75}Al_{24}M_1$ (where M = Ag, Au, Pd, and Pt) were manufactured in quartz crucibles in an induction furnace under inert atmosphere using elements with purity higher than 99.99%. The ingots were prepared by the fusion of stoichiometric amounts of the high-purity elements (solid rods), and the melt was homogenized by the convective currents generated by the induction furnace. After melting the metal elements, the ingots were allowed to cool to room temperature inside the induction furnace. From the ingots, samples were cut with dimensions of $20 \times 5 \times 2$ mm to carry out the tests.

XRD analysis of alloys was carried with a Bruker D8 Advance diffractometer equipped with a Cu Kα ($k = 1.5418$ Å; 40 kV) monochromatic source and a LYNXEYE$^{\text{TM}}$ 1D positional detector. Scans were performed from $2\theta = 5°$ to $100°$ with a $0.02°$ step and an irradiation time of 0.2 seconds.

In order to reveal the microstructure of the intermetallic alloys, they were etched by immersing in HF-HNO$_3$ solution (1 : 1 molar ratio) for 5 to 10 seconds at room temperature.

For the oxidation test, samples were grinded with a silicon carbide paper to 600-grit size, washed with water, and ultrasonically cleaned with acetone. In order to have a larger reaction area, two samples were employed in each test: one was used for surface analysis and the other for cross-sectional analysis.

Oxidation tests were carried out in pure oxygen at 900, 1000, and 1100°C. This range was chosen since at these temperatures, there is a change in the stability of the different
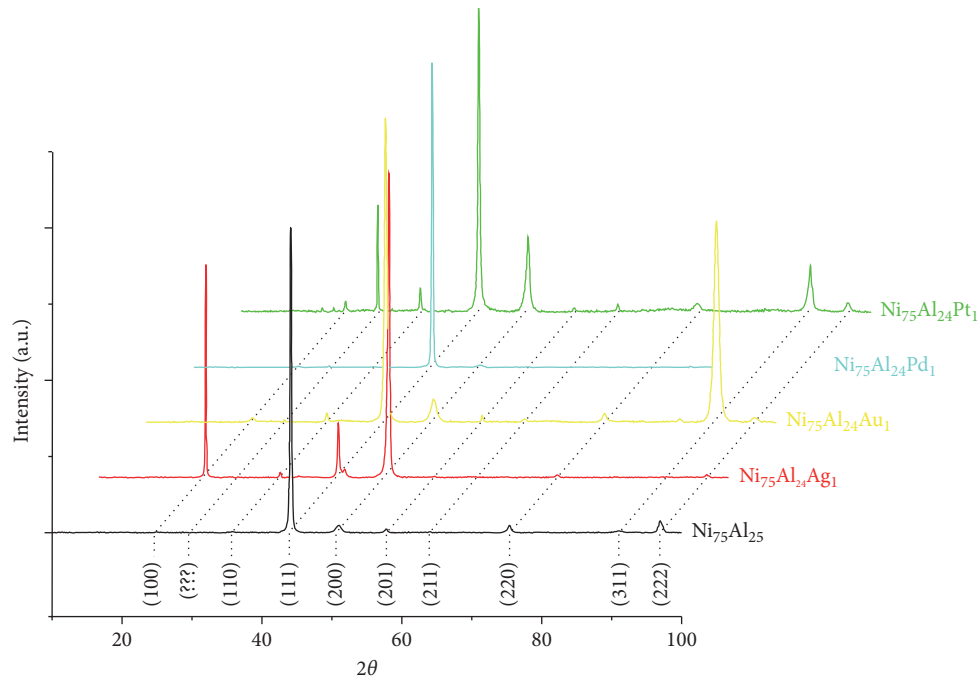
FIGURE 1: The XRD patterns of Ni$_3$Al and Ni$_3$Al doped with 1 at.% of noble metals.

phases of Al$_2$O$_3$; at 900°C, transition between γ-phase and θ-phase begins; at 1000°C, θ-phase is stable; and at 1100°C, α-phase is stable. Before each test, the electric furnace was preheated to the experimental temperature. The record of the weight gain curves as a function of exposure time was done with a thermobalance CI MK2-M5 Head LM 2-01 and the LabWeigh software. Analyses were carried out by means of a scanning electron microscope (Zeiss model DSM 960) and the energy dispersive X-ray analysis (EDXA).

3. Results and Discussion

3.1. XRD Analysis of Alloys. The XRD profiles of the alloys with and without noble metal additions are shown in Figure 1. The XRD profile of the Ni$_3$Al alloy shows the characteristic peaks (111), (200), (220), (311), and (222) corresponding to the L_{12} superstructure (γ'-phase), and their relative intensities are consistent with previous reports [38–40], which indicate a complete transformation from metals to the Ni$_3$Al intermetallic alloy.

The peaks observed in the XRD profiles of the doped alloys are wide, suggesting a small crystallite size. In addition, the intensities of some peaks increase and decrease depending on the added noble metal. The Ni$_{75}$Al$_{24}$Ag$_1$ profile shows highest intensities in (100) and (200), and the intensity of the peak decreased in (111); this suggests the crystal growth in two preferential planes. This preferential growth was also observed in the Ni$_{75}$Al$_{24}$Pd$_1$ alloy, where the profile shows a slight increase in the (222) peak, indicating a preferential unidirectional growth [41]. The XRD profile for the Ni$_{75}$Al$_{24}$Au$_1$ alloy shows a notable increase in the intensity of the (311) peak and a slight increase in the intensity of the (200) peak, and the characteristic peak (111) shows no change. On the other hand, the XRD profile of the

Ni$_{75}$Al$_{24}$Pt$_1$ alloy shows an increase in the intensity of all its peaks, and an unidentified peak at $2\theta = 29.56$ is observed. Considering that the positions of the atoms in the unit cell affect the intensities but not the directions of the diffracted beams [42], the change in peak intensities can be completely attributable to the addition of noble metals.

Properties such as hardness show a significant dependence on crystallographic planes: for Ni$_3$Al, the highest value occurs in (100), followed by (111) and (110) [43]. However, several studies about the Ni$_3$Al oxidation indicate that there are no significant differences in the oxidation behavior between planes (100), (110), and (111) [44–48]. Taking into account that the planes (100) and (110) consist of a series of two layers: the most stable having a composition of 50% Ni and 50% Al and the other with 100% Ni and the plane (111) having a composition of 75% Ni-25% Al [49, 50]; then due to it, it is possible the presence of zones with different chemical compositions onto alloy surface (i.e., change in the Al/Ni ratio). In addition, substitution at preferential sites by the addition of noble metals can further change the surface chemical composition, thereby greatly influencing its oxidation behavior.

3.2. Microstructural Analysis. Figure 2 shows the microstructure of the intermetallic Ni$_{75}$Al$_{25}$ alloy, where the presence of two phases is observed. The EDXA showed that the dendrite is a phase with high concentration of Al, so that the (γ-γ') phase is in the matrix and the (β-γ') phase is in the dendrite core as indicated by Hunziker and Kurz [51] and Rosas et al. [52], respectively. During the solidification process, there is no cooling rate sufficiently slow to maintain equilibrium in the melt; that is, there is insufficient time for the composition gradients to be diffusion removed and the dendrites retained [53]. Its formation also may be
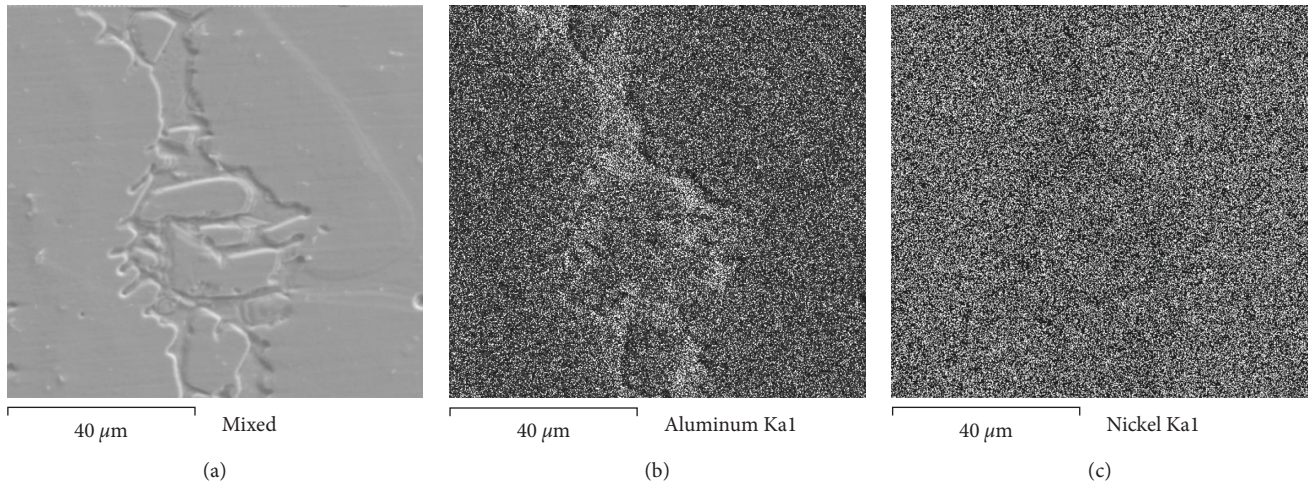
| 40 μm   Mixed | 40 μm   Aluminum Ka1 | 40 μm   Nickel Ka1 |
| (a) | (b) | (c) |

FIGURE 2: Microstructure of the $Ni_{75}Al_{25}$ intermetallic alloy (a) and EDXA mapping for Al (b) and Ni (c) of the dendrite structure.

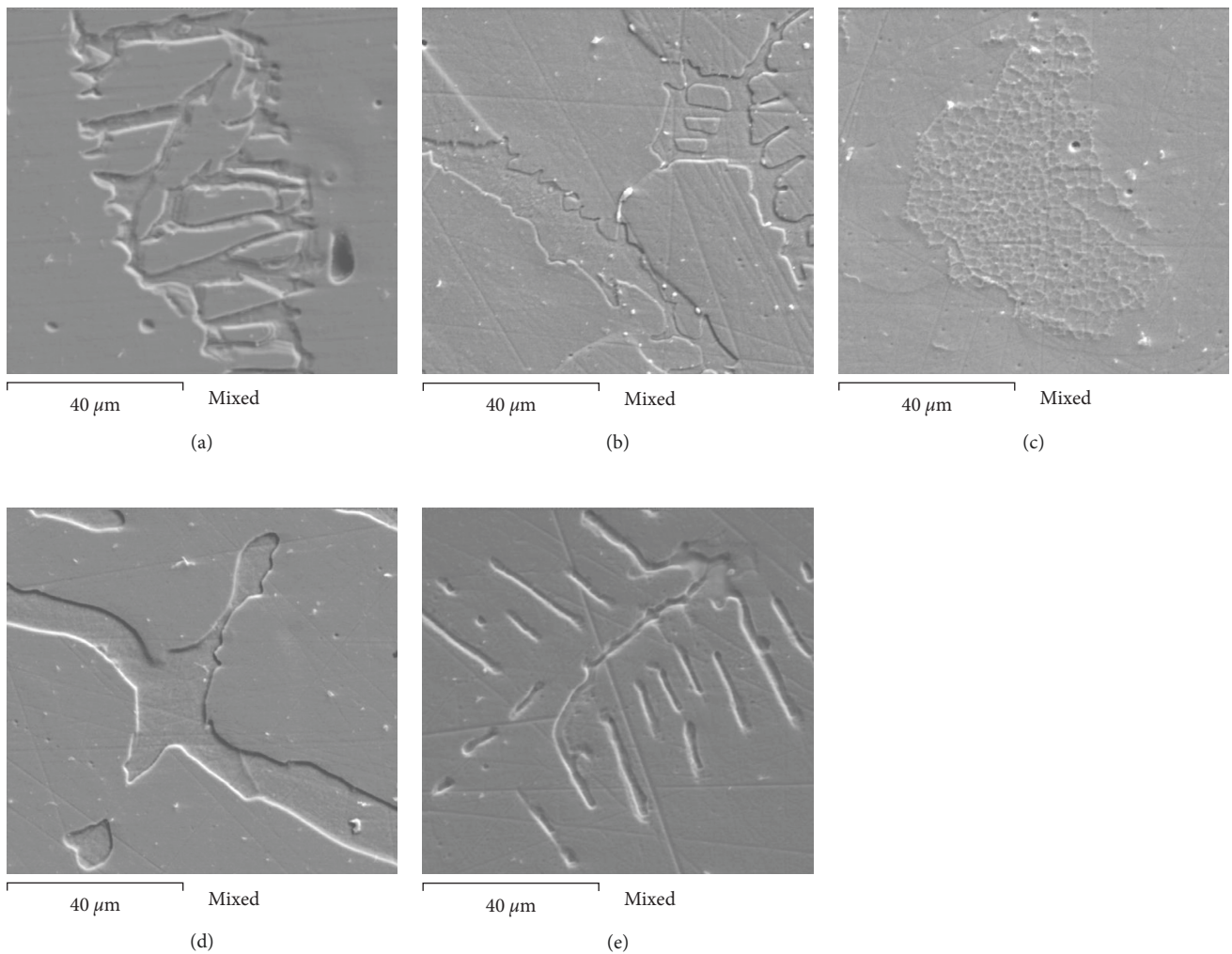| 40 μm   Mixed | 40 μm   Mixed | 40 μm   Mixed |
| (a) | (b) | (c) |

| 40 μm   Mixed | 40 μm   Mixed |
| (d) | (e) |

FIGURE 3: Microstructure of the Ni_3Al intermetallic alloys: (a) undoped, (b) 1.0% Ag, (c) 1.0% Au, (d) 1.0% Pd, and (e) 1.0% Pt.

attributable to the difference between the melting points of the constituent phases. According to Lee et al. [11, 17], when the solidification process begins, it is favored by the formation of the dendritic structures (β-γ'), and during the cooling process, the γ-phase decreases while the γ'-phase increases.

Figure 3 shows the microstructure of intermetallic alloys evaluated, and it is observed that there are notable changes in

TABLE 1: Spaces between secondary arms and space ratio, taking as reference the undoped alloy.

Alloy	Space between secondary arms (μm)	Space ratio between secondary arms with respect to Ni$_3$Al
Ni$_3$Al	47.00	1.00
Ni$_3$Al + 1% Ag	23.30	0.49
Ni$_3$Al + 1% Au	73.04	1.55
Ni$_3$Al + 1% Pd	17.07	0.36
Ni$_3$Al + 1% Pt	10.24	0.22

the microstructure of the doped alloys, which can be explained according to the preferential growth plane of each alloy (Figure 1) and an increase in the solidification rate. The dendrite structure of Ni$_{75}$Al$_{25}$ (Figure 3(a)) has a spacing between secondary arms of 47 μm, and this value is typical in a conventional solidification process [54]. The space between the secondary arms of the dendrites is inversely related to the cooling rate during the solidification process, which has been correlated according to the following equation [55]:

$$d_2 = kv^{-1/3},\tag{1}$$

where d_2 is the secondary dendrite arm spacing, v is the solidification cooling rate, and k is a constant of the alloy.

Since the solidification cooling rate is inversely proportional to the space between the secondary arms of the dendrites, from Table 1, it can be noticed that the solidification cooling rate in the Ni$_{75}$Al$_{24}$Pd$_1$, Ni$_{75}$Al$_{24}$Pt$_1$, and Ni$_{75}$Al$_{24}$Ag$_1$ alloys was faster than in the Ni$_{75}$Al$_{25}$ alloy, so that there is a lower space between the secondary dendrite arms; moreover, several directions of dendrites in the Ni$_{75}$Al$_{24}$Pt$_1$ alloy are congruent with its preferential growth plane. This same affirmation is consistent with the Ni$_{75}$Al$_{24}$Pd$_1$ alloy with almost only one preferential growth plane. The solidification cooling rate in the Ni$_{75}$Al$_{24}$Au$_1$ alloy was slower than the undoped alloy such that the dendrites almost disappeared.

It is observed that the addition of Ag favors an increase in the ratio γ-γ'/β due to the reduction in the number and volume of the interdendritic phase (Figure 3(b)). Because of the low solubility of Ag in Ni [56], it is possible to observe the presence of Ag-rich phases. According to Zhou and Guo [57, 58], the presence of Ag at grain boundaries begins during the solidification process since this element segregates at the solid-liquid interface, and at the same time, the Ag solubility decreases causing their precipitation into the grains. The microstructure of the Au-doped intermetallic alloy showed a honeycomb appearance (Figure 3(c)); that is, there is not a tendency to form precipitates as in the case of Ag-doped intermetallic alloy. Sheng et al. [59] found that the effect of addition of 1% Au on the microstructure of the NiAl intermetallic alloy causes a grain size reduction and the formation of α-AlAu$_2$ precipitates. It can be assumed that the absence of the α-AlAu$_2$ phase is due to the lower content of Al in Ni$_3$Al compared to that in NiAl. Figures 3(d) and 3(e) show the microstructure of the intermetallic alloy doped with Pd and Pt, respectively. The Pd-doped alloy has dendritic structures

of bigger area; however, the relationship γ-γ'/β is much greater than in the alloy doped with Ag and Au, indicating that, at room temperature, the γ-γ' phase is stable. The Pt-doped alloy has very fine dendritic formations in which there is no enrichment of Al. In both cases, a uniform distribution of Pd and Pt is observed as in the case of the Au-doped intermetallic alloy. Meng et al. [60] indicate that the addition of Pd into Ni$_3$Al intermetallic alloy generates an increase of delocalized bonding electrons, and this causes a strengthening of the grain boundaries and improves the ductility of the alloy. Furthermore, Li et al. [61, 62], Oquab and Monceau [63], and Zhang et al. [64] mention that Pd plays an important role in stabilizing the β-phase in NiAl at high temperatures; the same effect is attributed to the addition of Pt [10]. No precipitates were observed in the interdendritic region of the alloys, indicating that the phases found there are results of a eutectic reaction, contrasting with the work of Lee et al. [11], which presents cell interdendritic microstructures that Hunziker and Kurz [5] defined as peritectic structures.

3.3. Oxidation Kinetics.
Figure 4 shows the curves (solid lines) of weight gain per unit area as a function of exposure time during the process of oxidation of the intermetallic alloys between 900 and 1100°C. The curves were fitted (dashed lines) to an equation of the form [24, 65]:

$$\Delta m = kt^n,\tag{2}$$

where Δm is the weight gain per unit area, k is the oxidation rate constant, n is the exponent of velocity, and t is the time of exposure. The values of k and n to fit the experimental results are shown in Table 2. Adjustments were done using a nonlinear least-squares regression method (Gauss–Newton method) [66]. According to the n values obtained, it can be observed that only at 900°C, the oxidation kinetics of the Ni$_3$Al alloy and the Ag-doped alloy follows a parabolic behavior, all other n values correspond to a subparabolic behavior. The oxidation mechanism of a protective oxide that grows with parabolic kinetics mainly consists of the diffusion of cations from the metal-oxide interface to the oxide-gas interface; however, when the oxidation mechanism approaches to cubic kinetics, some authors attribute this behavior to the oxide grain growth [67, 68], although other authors claim that the formation of a protective layer like α-Al$_2$O$_3$ is more a rule than an exception [69]. An additional characteristic of the subparabolic kinetics is that at the beginning of the oxidation process, a great weight gain is observed with respect to that observed in a parabolic kinetic, being this a characteristic of the transient stage of the oxidation process.

At 900°C, Ag- and Au-doped alloys had the highest weight gain throughout the exposure period with respect to the undoped alloy, whereas Pd- and Pt-doped alloys had the lower weight gain. During first two hours, the Au-doped alloy has a significantly greater weight gain, while Ag-, Pd-, and Pt-doped alloys have a similar and slightly higher weight gain than the undoped alloy. At 1000°C, all doped alloys (except Pd-doped alloy) have the greater
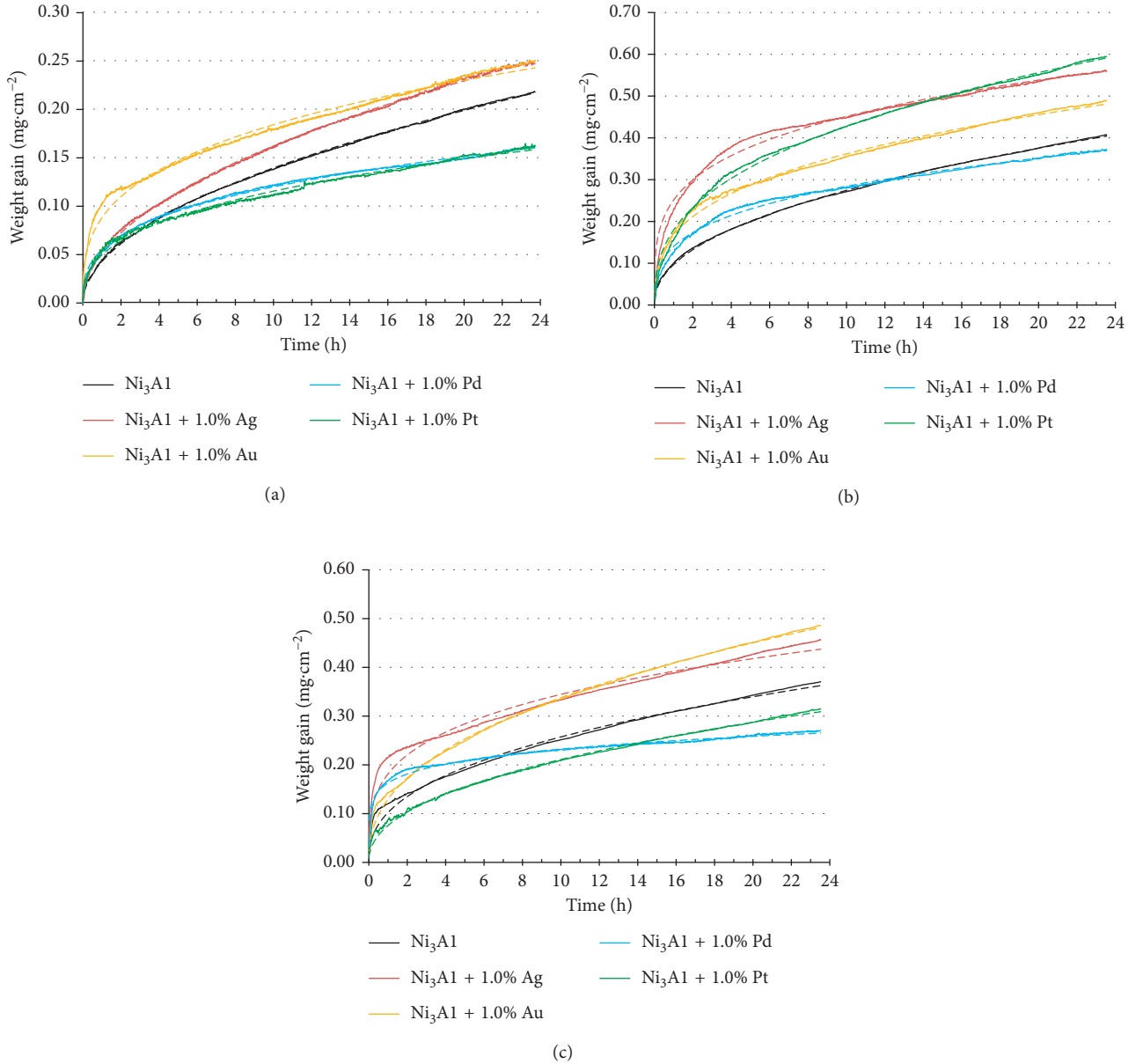
(a)

(b)

(c)

FIGURE 4: Weight gain of intermetallic alloys oxidized in O_2 at (a) 900°C, (b) 1000°C, and (c) 1100°C.

TABLE 2: Values of k and n obtained from the curves of weight gain.

Temperature (°C)		Ni_3Al	$Ni_3Al + 1.0\%$ Ag	$Ni_3Al + 1.0\%$ Au	$Ni_3Al + 1.0\%$ Pd	$Ni_3Al + 1.0\%$ Pt
900	k	0.0430	0.0513	0.0879	0.0553	0.0497
	n	0.5106	0.4998	0.3199	0.3350	0.3653
1000	k	0.0971	0.2515	0.1684	0.1402	0.1799
	n	0.4517	0.2541	0.3323	0.3070	0.3769
1100	k	0.1022	0.1814	0.1297	0.1604	0.0755
	n	0.4009	0.2785	0.4156	0.1602	0.4460

weight gain with respect to the undoped alloy, in a decreasing order of Au-, Ag-, and Pt-doped alloys. This behavior may be because the doped alloys stabilize the θ-Al_2O_3 phase and therefore reduce the α-Al_2O_3 phase transformation as Pt does according to Cadoret et al. [70]

and Hayashi and Gleeson [71]. The θ-Al_2O_3 phase generates more pathways for diffusion because of its smaller grain size compared to α-Al_2O_3 phase. The k values at 1000°C show magnitudes that explain the high increase in weight gain for doped alloys. At 1100°C, there is a clear grouping in
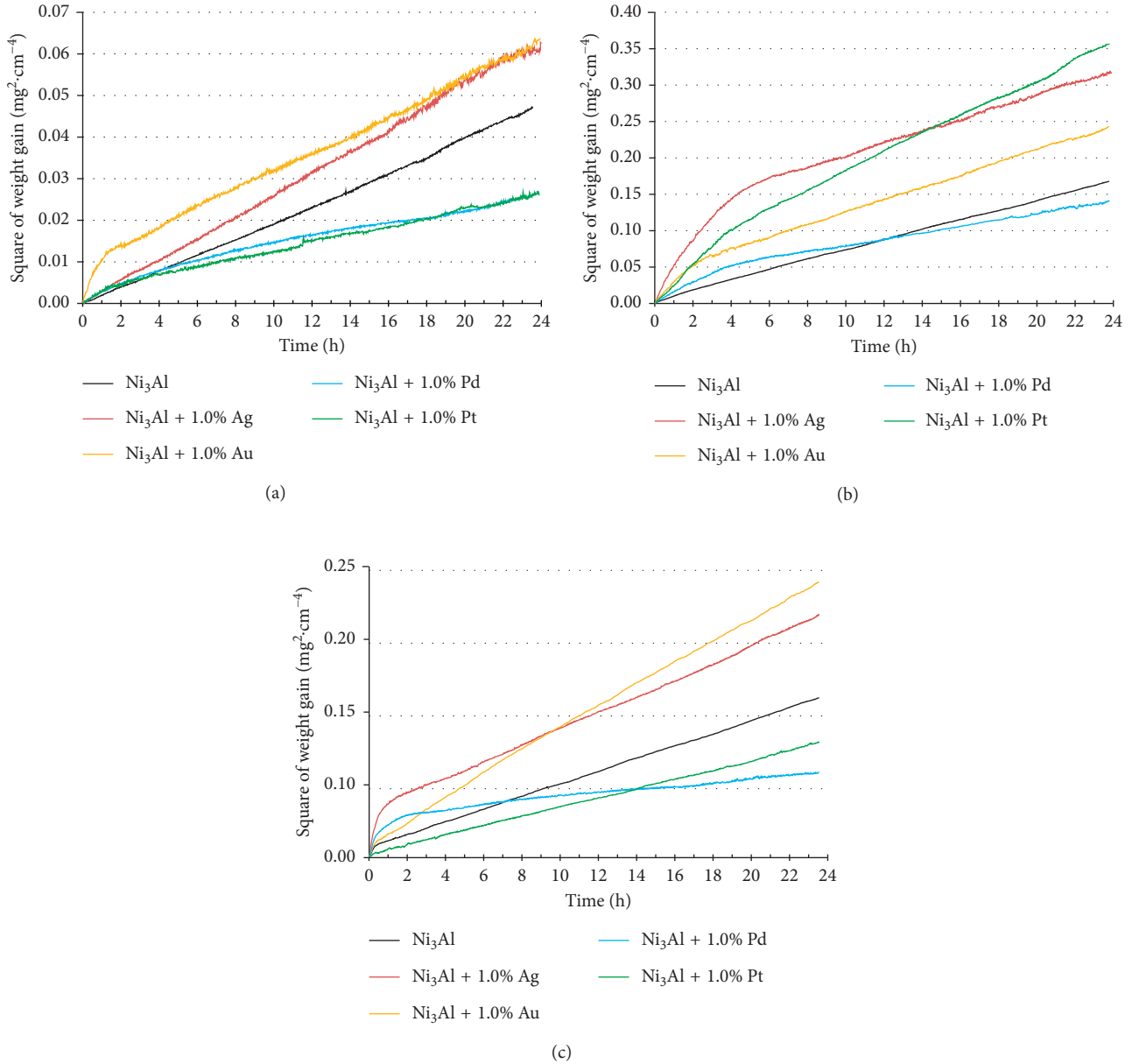
FIGURE 5: Square weight gain versus time of exposure of intermetallic alloys oxidized in O_2 at (a) 900°C, (b) 1000°C, and (c) 1100°C.

terms of weight gain between the Pd- and Pt-doped alloys (lowest) and the Ag- and Au-doped alloys (higher) compared to undoped alloy, similar as at 900°C. The Pt-doped alloy has the lower weight gain than the undoped alloy throughout the exposure period, while the Pd-doped alloy has a higher weight gain than the undoped alloy only in the first six hours. All alloys except Pd-doped alloy have a remarkably high weight gain in the first hour.

The weight gain curves of Figure 4 give an impression about the effect of the addition of noble metals in the oxidation process, but it is also necessary to know the rate of oxidation. Considering strictly a parabolic behavior $n = 0.5$, for comparative purposes (2) can be rewritten as

$$\Delta m^2 = k_p t, \qquad (3)$$

where k_p is the parabolic rate constant. The linearity of (3) allows graphically displaying and estimating the k_p value considering the slope of the $\Delta m^2 - t$ relationship. In Figure 5, changes in the parabolic rate constant showing two k_p values can be identified, the first k_p value being greater than the second one; this is due to the fact that it is mathematically forcing a curve with a subparabolic behavior to be adjusted to a parabolic behavior [69], so the k_p value that will be taken into account to characterize the oxidation process will be that of the second slope which is presented in Table 3.

At 900°C, undoped and Ag-doped alloys show a constant k_p value throughout the exposure period. The k_p value of Pd- and Pt-doped alloys is similar, and it is lower than that for the undoped alloy. At 1000°C, the k_p value of the Au-doped

TABLE 3: Values of k_p obtained from slopes of Figure 5.

Temperature (°C)	Ni$_3$Al	Ni$_3$Al + 1.0% Ag	Ni$_3$Al + 1.0% Au	Ni$_3$Al + 1.0% Pd	Ni$_3$Al + 1.0% Pt
900	0.0019	0.0026	0.0022	0.0010	0.0010
1000	0.0072	0.0082	0.0085	0.0045	0.0136
1100	0.0054	0.0071	0.0095	0.0016	0.0040

(a)

(b)

(c)
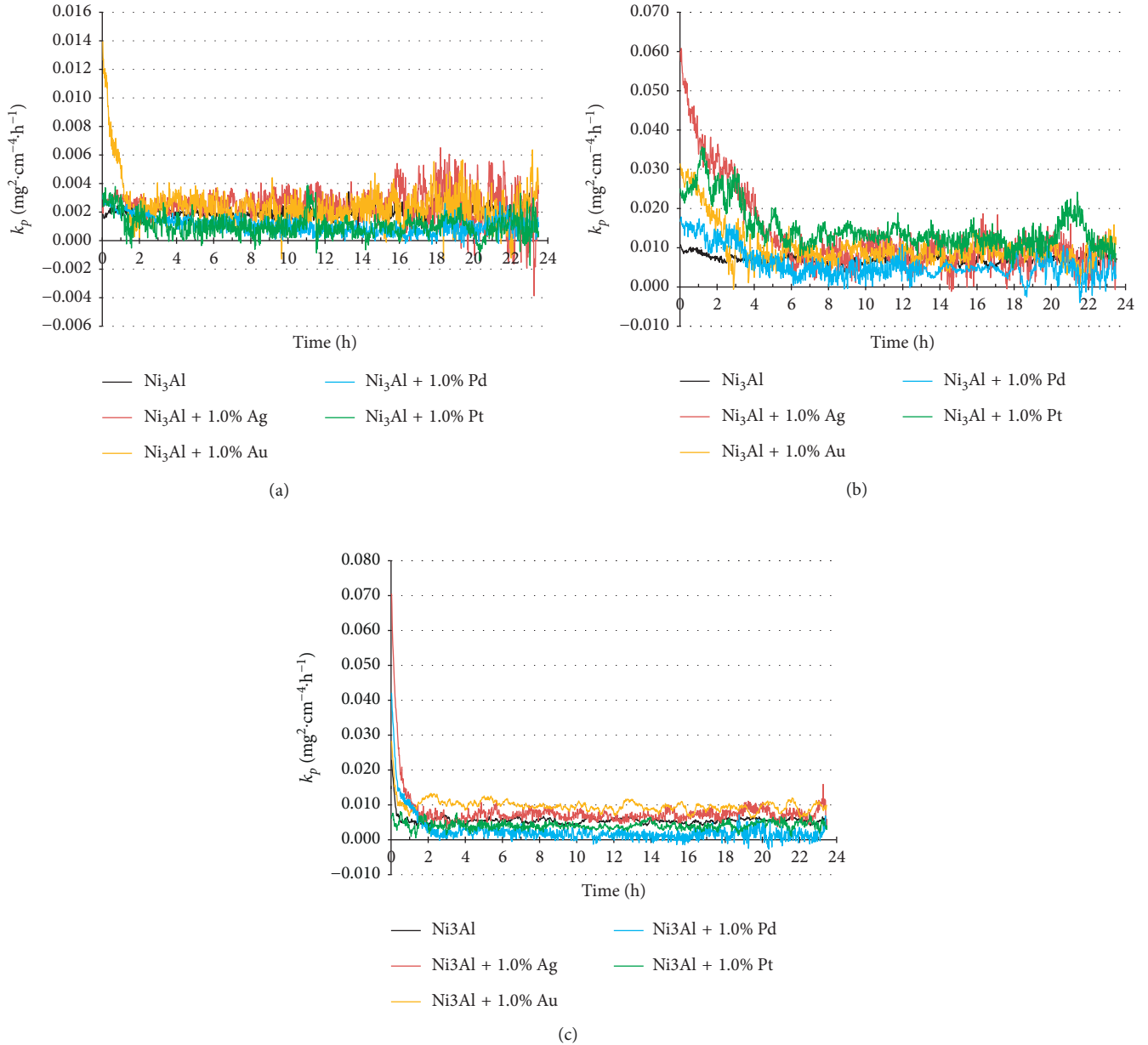
FIGURE 6: Instantaneous k_p versus time for the intermetallic alloys oxidized at (a) 900°C, (b) 1000°C, and (c) 1100°C.

TABLE 4: Average values of instantaneous k_p from Figure 6.

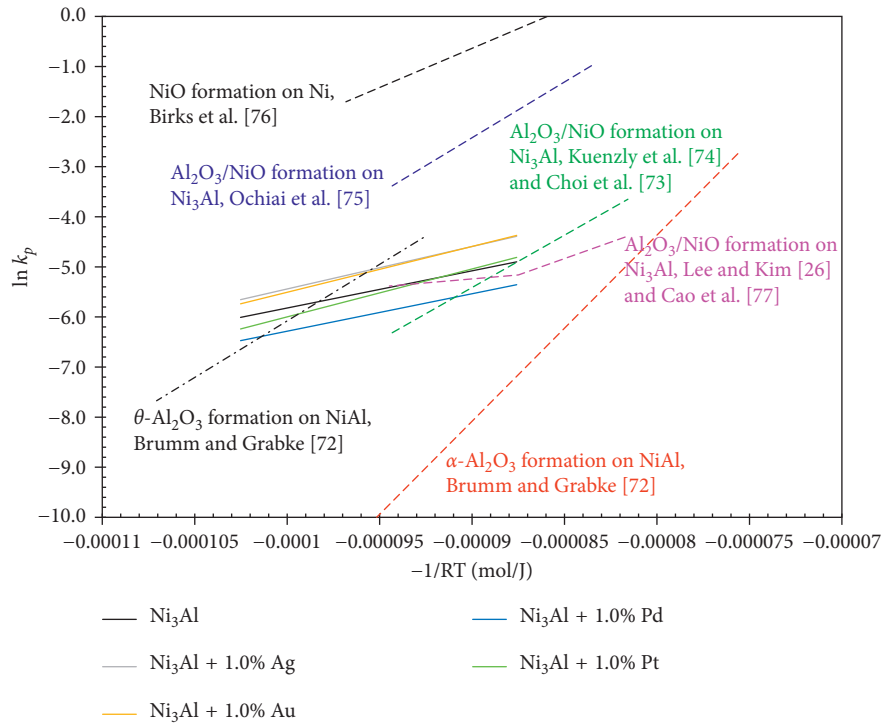| T (°C)	Ni$_3$Al	Ni$_3$Al + 1% Ag	Ni$_3$Al + 1% Au	Ni$_3$Al + 1% Pd	Ni$_3$Al + 1% Pt
900	0.0020	0.0026	0.0027	0.0011	0.0011
1000	0.0070	0.0132	0.0102	0.0059	0.0149
1100	0.0058	0.0088	0.0101	0.0032	0.0041

FIGURE 7: Arrhenius graph showing the k_p variation in function of temperature.

TABLE 5: Values of k_0 and Q obtained from the Arrhenius graph.

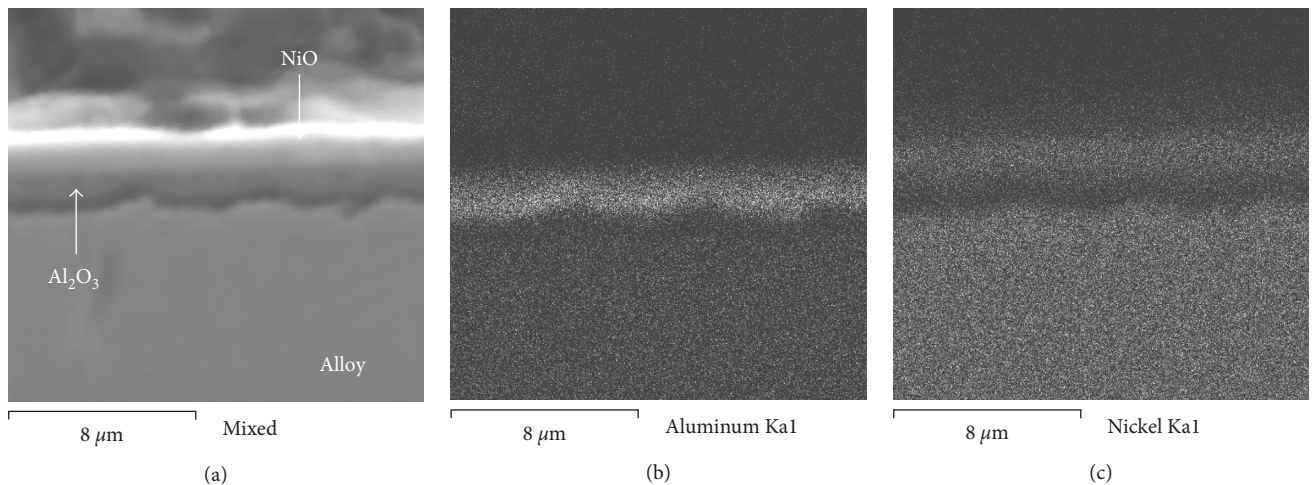|	Ni₃Al	Ni₃Al + 1.0% Ag	Ni₃Al + 1.0% Au	Ni₃Al + 1.0% Pd	Ni₃Al + 1.0% Pt
$\ln(k_0)$	1.6031	3.0341	3.6400	1.1934	3.5693
Q (kJ/mol)	74.2443	84.7525	91.4718	74.7778	95.6762

FIGURE 8: SEM micrograph (a) and mapping elements (b, c) of the scale formed onto Ni₃Al at 900°C.

alloy decreases at three hours after starting the test, the k_p value of Ag, Pd, and Pt doped alloys decreases at four hours after starting the test, while for the undoped alloy, its k_p value remains constant. At 1100°C, the k_p value of the undoped and doped alloys decrease at the first half an hour after starting

the test, except the Pt-doped alloy, for which the k_p value remains constant. In most alloys, at all temperatures, it is observed at most only one change in k_p, except the Pd-doped alloy at 1100°C with two changes: half an hour and two hours after starting the test. At 1000°C, the k_p value of the
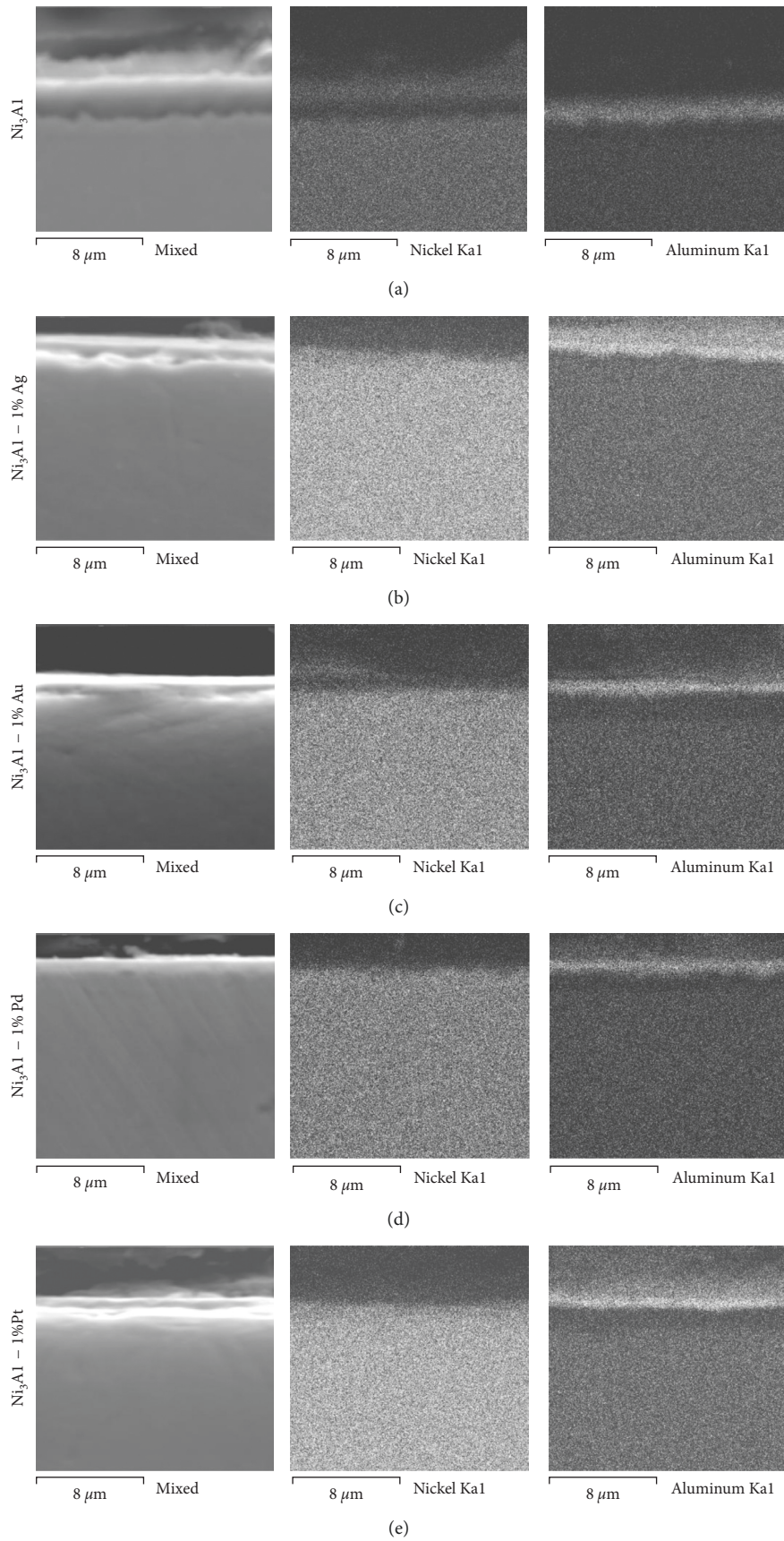
(a)

(b)

(c)

(d)

(e)

FIGURE 9: Cross section of intermetallic alloys and mapping elements after oxidation at 900°C: (a) Ni$_3$Al, (b) Ag-doped alloy, (c) Au-doped alloy, (d) Pd-doped alloy, (e) Pt-doped alloy.
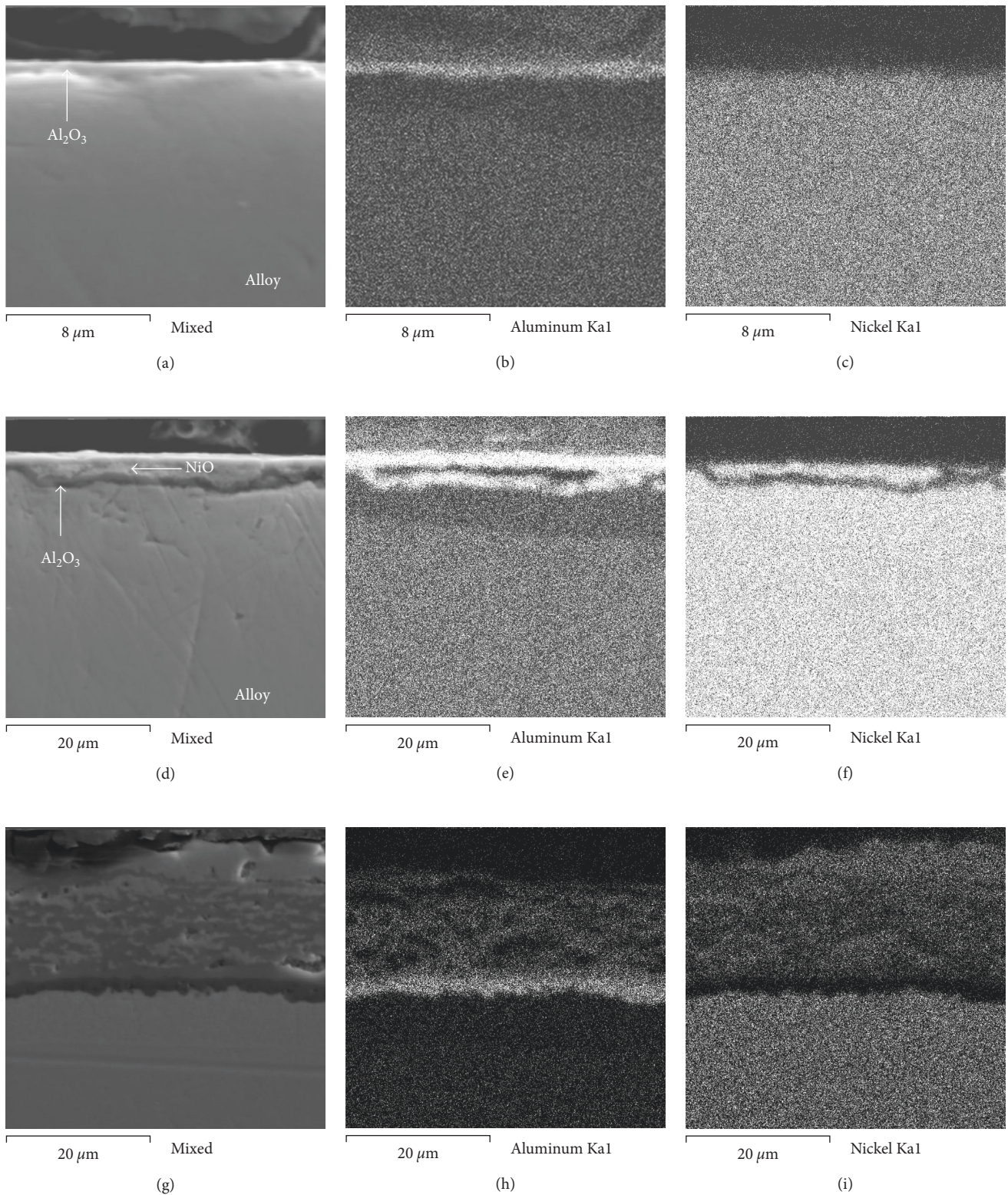
Figure 10: SEM micrograph and mapping elements: (a–c) Pd-doped alloy (900°C), (d–f) Pt-doped alloy (1000°C), and (g–i) Ag-doped alloy (1100°C).

Au-doped alloy decreases at three hours after starting the test, and for Ag-, Pd-, and Pt-doped alloys, the k_p value decreases at four hours after starting the test, while for the undoped alloy, its k_p value remains constant. At 1100°C, the k_p value of all alloys (except Pt) decreases after 30 min, and for Pt-doped alloy, the k_p value remains constant.

When it is not possible to obtain accurate measurement from the slopes, it is necessary to consider the average of the
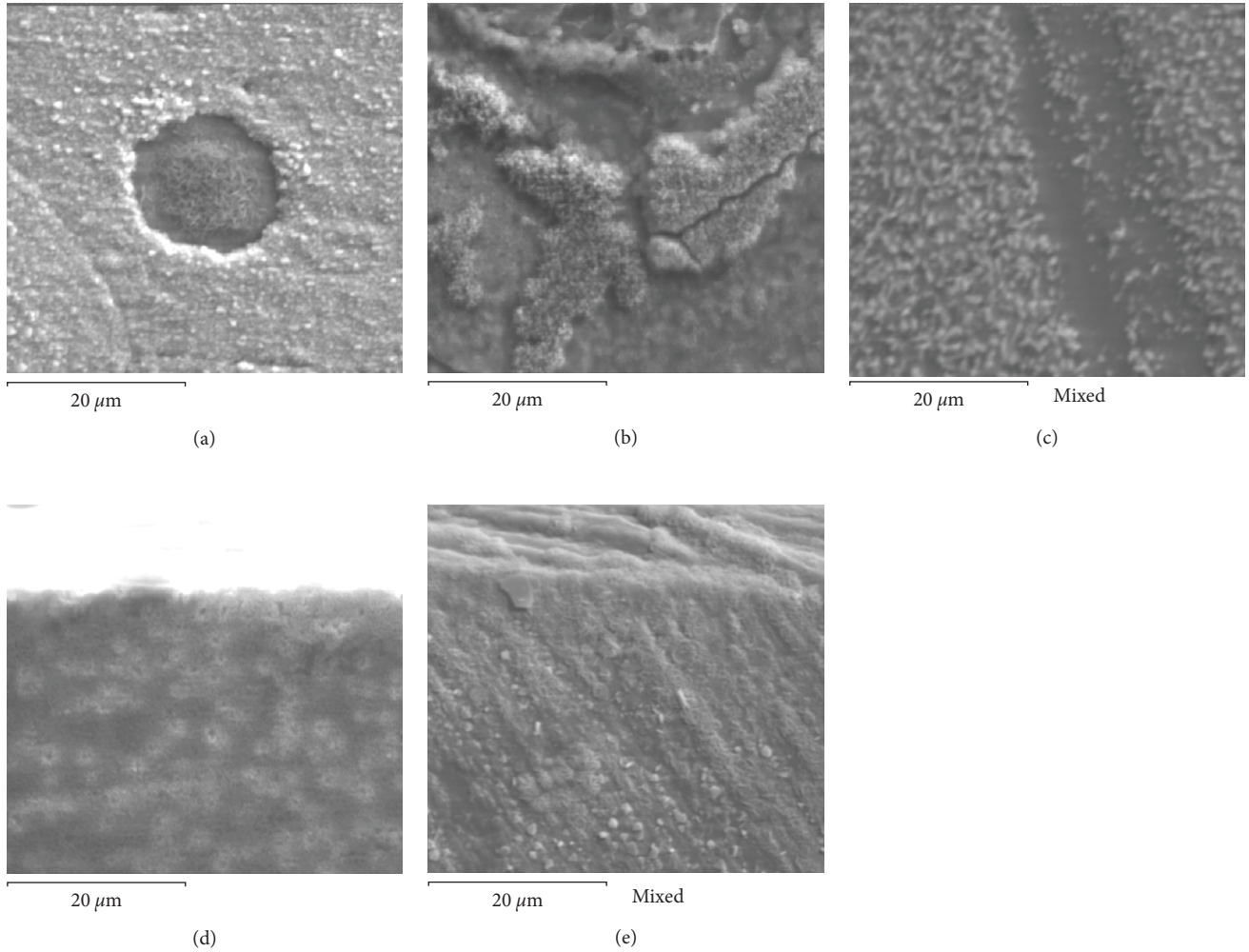
FIGURE 11: SEM micrographs showing the surface morphology of the oxide scales at 900°C: (a) Ni_3Al, (b) $Ni_3Al + 1.0\%$ Ag, (c) $Ni_3Al + 1.0\%$ Au, (d) $Ni_3Al + 1.0\%$ Pd, and (e) $Ni_3Al + 1.0\%$ Pt.

instantaneous parabolic constants, which results in differentiating (3) versus time [65],

$$\frac{d\left(\Delta m^2\right)}{dt} = k_p. \tag{4}$$

The instantaneous parabolic constant (k_p) of the oxidation tests is shown in Figure 6. This type of representation of the experimental data provides more information regarding the evolution of oxidation rates. At 900°C (Figure 6(a)), in the first two hours, the k_p values of the Au-doped alloy decrease seven times its equilibrium value, while in the Pd- and Pt-doped alloys, the k_p values decrease two times their equilibrium value; on the other hand, the Ag-doped alloy and undoped alloy maintain a constant rate. At 1000°C (Figure 6(b)), it is observed that the values of the instantaneous parabolic constant k_p of doped alloys tend to decrease in the first 6 hours, and then they remain constant, and for the undoped alloy, the k_p values remain constant. For the Ag-doped alloy, its k_p value decreases six times its equilibrium value, and for other doped-alloys, their k_p values decrease two times their equilibrium value. Finally, at 1100°C (Figure 6(c)), the

Pt-doped alloy shows a stable behavior, and the other alloys show a fast decrease in their k_p values in the first hour.

In order to visualize the effect of the temperature on the rate constants, it is necessary to determine the activation energy of the oxidation process from the Arrhenius equation.

$$\ln k_p = \ln k_0 - Q \cdot (RT)^{-1}, \tag{5}$$

where Q is the activation energy, R is the universal gas constant, T is the temperature, k_p is the rate constant, and k_0 is the preexponential factor. Plotting $\ln k_p$ versus $-(RT)^{-1}$ from the slope of the lines, the Q value can be determined. Perez et al. [65] suggest assuming a parabolic kinetics in the whole temperature range; therefore, the average value of instantaneous k_p from Figure 6 was calculated. Table 4 shows the average values of instantaneous k_p.

In order to compare the results of this work, Figure 7 shows the instantaneous k_p values obtained along with those reported in other studies. At 900 and 1000°C, the k_p values of both doped and undoped alloys tend to k_p values where the formation of the θ-Al_2O_3 phase may be possible in NiAl as reported by Brumm and Grabke [72]. At 1100°C, the k_p values are concentrated at a point between the formation of
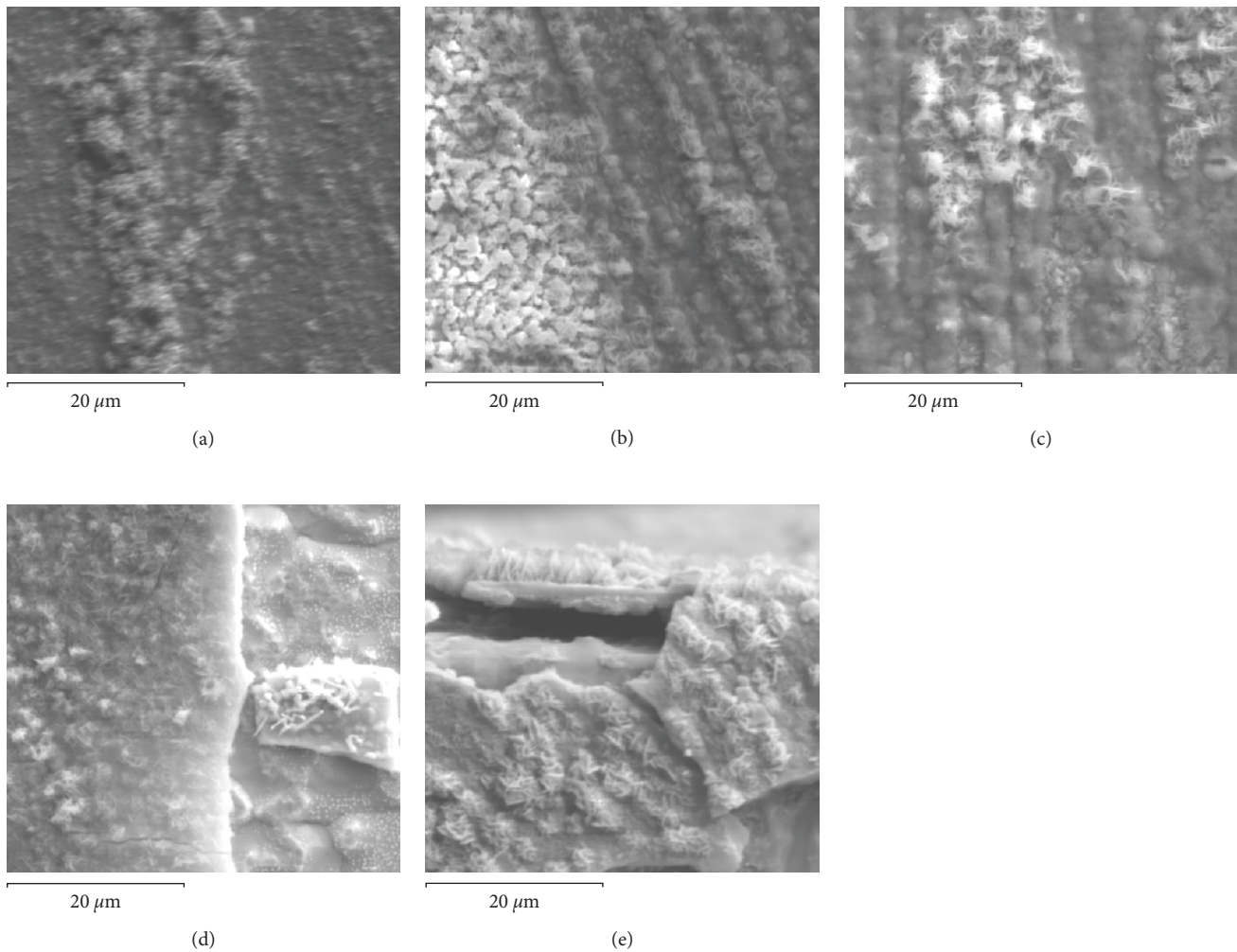
(a)

(b)

(c)

(d)

(e)

FIGURE 12: SEM micrographs showing the surface morphology of the oxide scales at 1000°C: (a) Ni$_3$Al, (b) Ni$_3$Al + 1.0% Ag, (c) Ni$_3$Al + 1.0% Au, (d) Ni$_3$Al + 1.0% Pd, and (e) Ni$_3$Al + 1.0% Pt.

θ-Al$_2$O$_3$ and α-Al$_2$O$_3$; an explanation for this behavior could be that, at this temperature, the stability of the α-Al$_2$O$_3$ begins [18] and this tends to decrease the weight gain [70, 71]. At 900°C and 1000°C, the k_p value of the undoped alloy is similar to results reported by Lee and Kim [26] and Choi et al. [73], and at 1100°C, it is similar to results of Kuenzly et al. [74]. The Pt-doped alloy has k_p values similar to the undoped alloy, Ag- and Au-doped alloys have higher k_p values, and the Pd-doped alloy has lower k_p values.

Activation energy is an important parameter that characterizes the predominant oxidation mechanism [75]; for example, the results presented by Ochiai et al. [75] and Kuenzly et al. [74] suggest that, in both cases, the oxidation mechanism is similar, although the experimental conditions were different, that is, cyclic oxidation tests and continuous oxidation tests. On the other hand, analyzing the results for the formation of α-Al$_2$O$_3$ scale [72] and NiO scale [76], it is observed that the preexponential factor is inversely proportional to the protective capacity of the protective oxide. Table 5 shows the activation energies and preexponential factors obtained from the Arrhenius graph (Figure 7). The activation energy value of Ni$_3$Al is similar to those values

reported by Lee and Kim [26] and Cao et al. [77], but almost three times lower than that reported by other authors [73, 74]. This difference is because the intermetallic alloy used in this study was not thermally treated. Activation energy values of the doped alloys show that the additions of the noble elements affect the Ni$_3$Al oxidation mechanism in the following order: Pt > Au > Ag > Pd. On the other hand, the Pd-doped alloy showed the lowest value of the preexponential factor.

3.4. SEM Analysis. SEM analysis showed that the oxide scale formed on all alloys had nonuniform thicknesses. In the case of Ni$_3$Al, the average thicknesses observed were between 2.44 and 2.86 μm in the temperature range studied. At 900°C (Figure 8), a double-layer oxide was developed, an outer Ni-rich layer and an internal Al-rich layer, with similar thicknesses. Other authors have described similar results [78]. However, at higher temperatures, only the presence of an Al-rich oxide was detected.

In general, the thickness of the oxide layer developed onto doped alloys was lower than that observed onto Ni$_3$Al.

20 μm   Mixed

(a)

20 μm

(b)

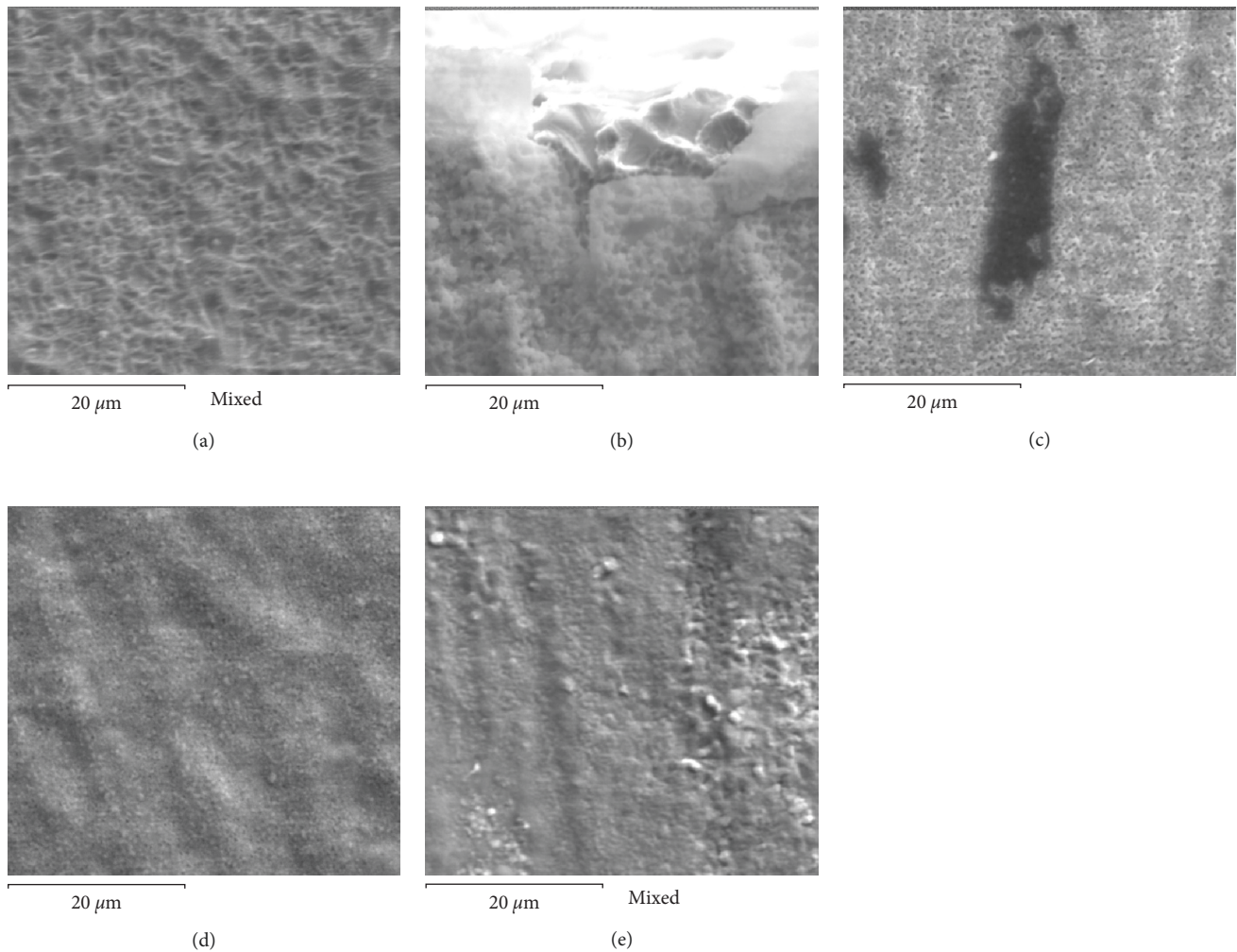20 μm

(c)

20 μm

(d)

20 μm   Mixed

(e)

FIGURE 13: SEM micrographs showing the surface morphology of the oxide scales at 1100°C: (a)Ni$_3$Al, (b)Ni$_3$Al + 1.0% Ag, (c) Ni$_3$Al + 1.0% Au, (d) Ni$_3$Al + 1.0% Pd, and (e) Ni$_3$Al + 1.0% Pt.

At 900°C, the average thicknesses were between 0.98 and 1.5 μm, at 1000°C, between 2.13 and 2.20 μm (except the Pt-doped alloy, its average thickness was 4.61 μm), and at 1100°C, between 1.43 and 2.55 μm (except the Ag-doped alloy, its average thickness was 4.52 μm). Figure 9 shows the thickness of the oxide formed on the intermetallic alloys oxidized to 900°C; similar aspects were observed at higher temperatures. At all test temperatures, the Pd-doped alloy showed the oxide layer with the lowest thickness (Figure 10(a)). In general, all doped alloys developed an Al-rich monolayer oxide (Figures 10(a)–10(c)), as has been reported in other studies [79]. In the case of alloys doped with Pt (at 1000°C) and with Ag (at 1100°C), zones with multilayer oxides and thicknesses up to 20 μm were observed (Figures 10(d) and 10(g)). In all cases, an Al-depleted zone was observed at the interface alloy oxide (Figures 8 and 10). This is due to the consumption of this element for the formation of protective oxide, Al$_2$O$_3$ [80]. Similar depletion processes have been reported in studies of corrosion by molten salts [81–85].

Figure 11 shows the surface morphology of the oxides formed at 900°C. The formation of oxides in the form of needles can be observed only onto nondoped alloy and onto those alloys doped with Ag and Au. This type of morphology is associated with the presence of the metastable phases of alumina [86–88], whose transformation from γ-Al$_2$O$_3$ to θ-Al$_2$O$_3$ occurs between 800 and 950°C [72]. It is worth mentioning that the alloys that presented this type of morphology had a greater weight gain (Figure 4(a)).

Figure 12 shows the surface morphology of the oxide scale at 1000°C. It is observed that, at this temperature, there is a greater presence of oxides in the form of needles (θ-Al$_2$O$_3$) both in the nondoped alloy and in those alloys doped with Ag, Au, and Pt. The alloy doped with Pd showed a lower presence of this phase, possibly due to a decrease in the growth rate of the θ-Al$_2$O$_3$ phase. Again, the surface morphology is correlated with the observed weight gain (Figure 4(b)); that is, the greater the presence of the θ-Al$_2$O$_3$ phase, the greater the mass gain.

On the other hand, the morphology of the oxides formed at 1100°C was completely different (Figure 13). In this case, the oxides formed show wrinkle shaped, which is characteristic of the α-Al$_2$O$_3$ phase [72]. This morphology is more evident in the nondoped alloy and in those doped with Ag
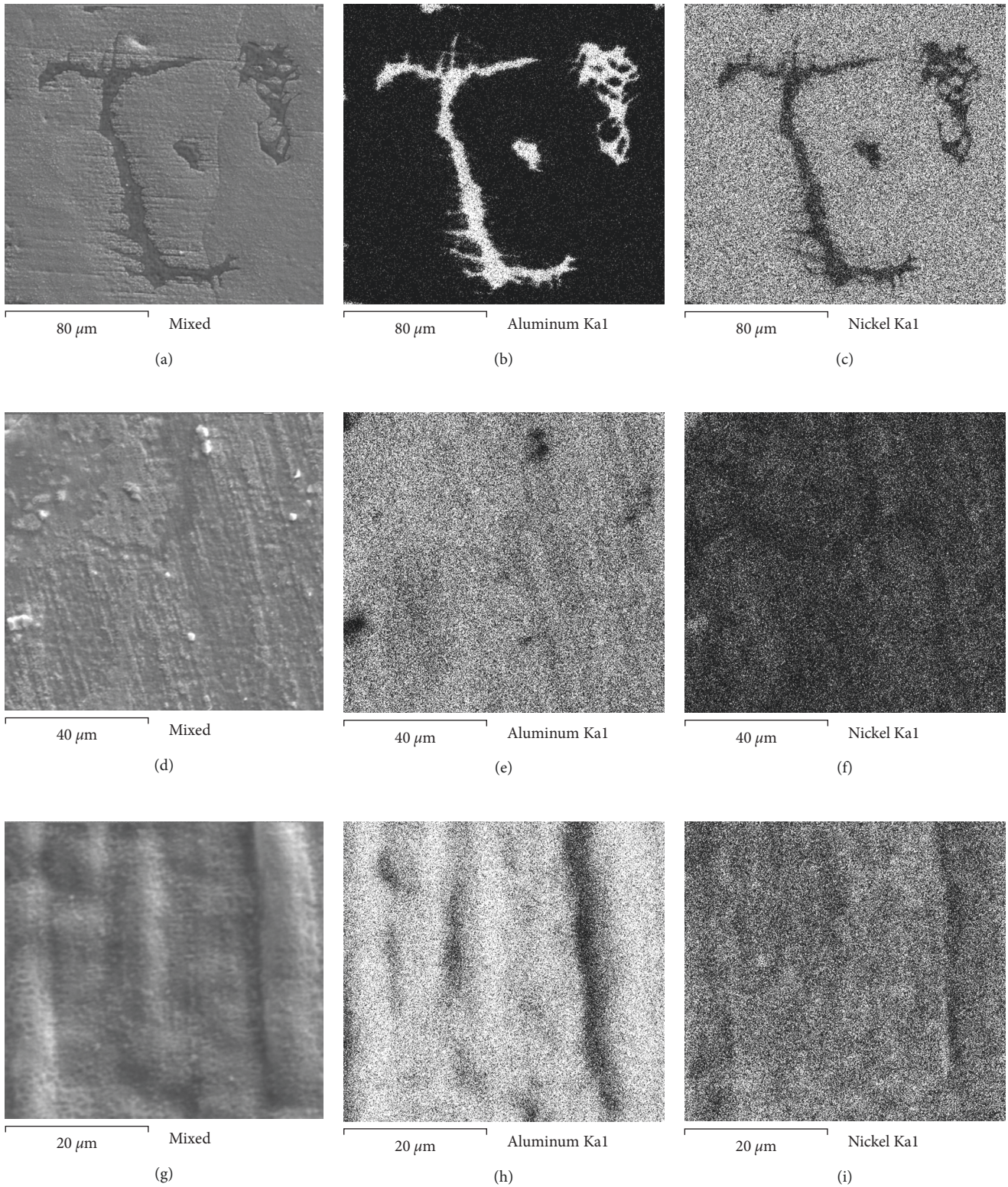
(a)

(b)

(c)

(d)

(e)

(f)

(g)

(h)

(i)

FIGURE 14: Superficial aspect and mapping elements of the oxide scale formed onto Ni_3Al at (a) 900°C, (d) 1000°C, and (g) 1100°C.

and Au, and in the alloys doped with Pd and Pt, a more compact and dense morphology was observed. These morphological differences indicate a difference in the growth rates of the oxide layers. In all cases, the weight gain at 1100°C was lower than that observed at 1000°C (Figure 4). This suggests that oxide layers rich in α-Al_2O_3 are more protective than those rich in θ-Al_2O_3.

Figure 14 shows the typical morphology of the Ni_3Al oxidized in oxygen for 24 hours. In general, a granular scale involving both heterogeneous Ni and Al oxides, mainly Ni
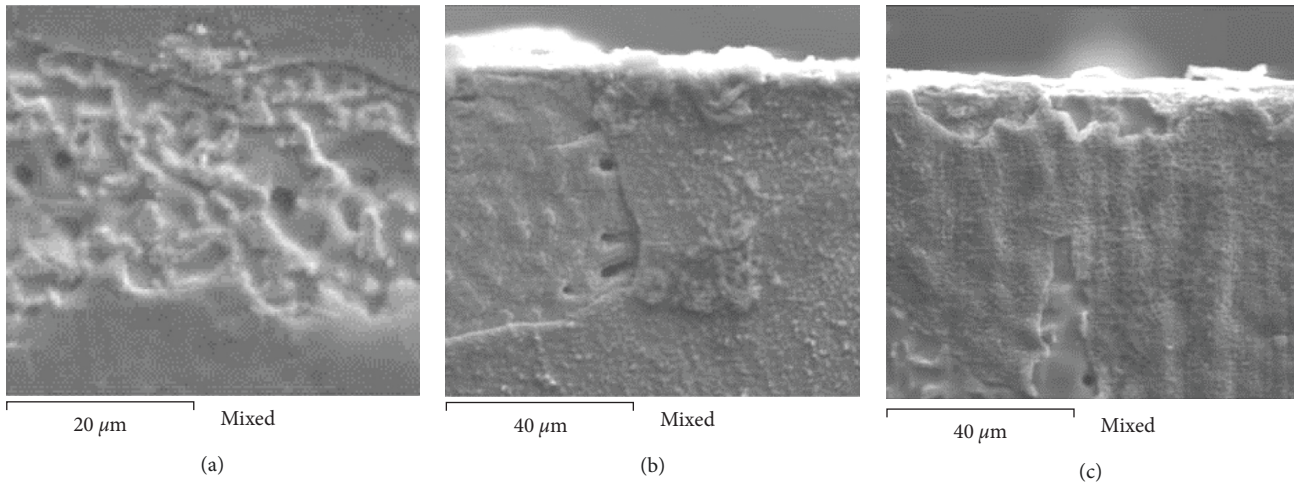
FIGURE 15: Cavities formed due to diffusion of Al during the oxidation process of the Ni$_3$Al in oxygen at (a) 900°C, (b) 1000°C, and (c) 1100°C.

oxides, as reported by Cao et al. [77] were observed. At 900°C, there are well-defined regions rich in Al$_2$O$_3$ which largely coincide with the interdendritic regions (Figure 14(a)). This suggests that the lateral growth of NiO could not fully cover the Al$_2$O$_3$, and the initial stage of oxidation occurred preferentially in the interdendritic phases [11]. At 1000 and 1100°C, the Ni$_3$Al surface was oxidized uniformly in comparison with the oxidized alloy at 900°C, but the surface mainly contains Al$_2$O$_3$ (Figures 14(d) and 14(g)). In some regions, the oxide layer has been cracked, probably during cooling, and it was possible to observe the presence of cavities into the scale-alloy interface (Figure 15). These sorts of cavities are formed by the consumption of Al and Ni in the course of formation of the oxide scale, and they have an impact on the adhesion of the scale [70].

The difference in the oxidation process between the dendritic and the interdendritic phases lies in the thermochemistry of alumina formation between the phases; that is, in the NiAl-rich dendritic phase, the following reaction may occur:

$$4NiAl + 3O_2 \leftrightarrows 2Al_2O_3 + 4Ni \ (\Delta G = -940.52 \ kJ @ 900°C) \tag{6}$$
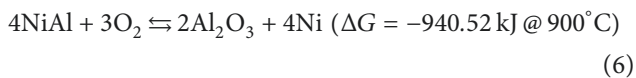
On the other hand, in the interdendritic phase where the Ni3Al phase predominates, the following reaction occurs:

$$4Ni_3Al + 3O_2 \leftrightarrows 2Al_2O_3 + 12Ni \ (\Delta G = -895.40 \ kJ @ 900°C) \tag{7}$$
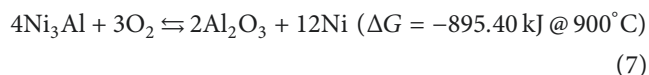
Thermochemically, the dendritic phase is more favored than the interdendritic phase. Considering also that in the doped alloys there is a considerable decrease in the dendritic phase (Section 3.2), it can be established that there exists a relation between the microstructural change and the thermochemical equilibrium conditions for the formation of an alumina layer. On the other hand, the absence of NiO in the surface of the doped alloys can also be attributed to the increase in the grain size of the Al$_2$O$_3$; that is, to say,

a decrease in the diffusion of Ni through the grain boundaries of the Al$_2$O$_3$ layer, which is related to the kinetics of subparabolic growth.

4. Conclusions

The XRD analysis of the alloys showed that the addition of 1% (atomic percent) of noble metals to the Ni$_3$Al intermetallic alloy promotes the preferential growth planes and increases the solidification rate by changing the microstructure of the base alloy. The oxidation behavior of doped alloys may be attributable to the change in the surface composition, taking into account that every growth plane has different compositions and that the preferential substitution site of the noble metals in the structure of Ni$_3$Al increases the Al/Ni ratio. In general, the addition of noble metals promotes the formation of oxide layers rich in Al$_2$O$_3$ and is evident that the diffusion of the Ni cations through Al$_2$O$_3$ scale is decreased, since the formation of NiO during the test time was not evident. Ag and Au additions increase the value of the parabolic rate constant k_p, while Pd and Pt decrease, the k_p values tend to values where the formation of θ-Al$_2$O$_3$ and α-Al$_2$O$_3$ is possible. The noble metal addition increased the activation energy value of the oxidation process compared to the nondoped Ni$_3$Al, except Pd. The low solubility of Ag and its low melting point caused microstructural localized failures into Ag-doped alloy.

Conflicts of Interest

The authors declare that they have no conflicts of interest regarding the publication of this paper.
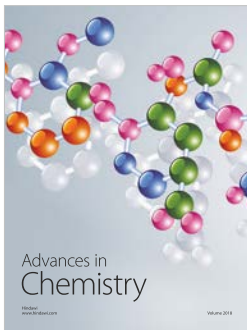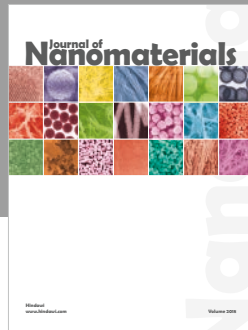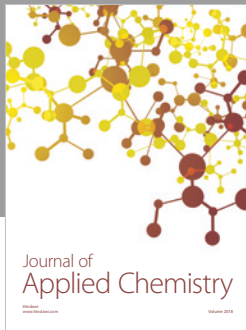
Acknowledgments

References

[1] S. C. Deevi and V. K. Sikka, "Nickel and iron aluminides: an overview on properties, processing, and applications," *Intermetallics*, vol. 4, no. 5, pp. 357–375, 1996.

[2] A. S. Verin, "Certain features of the structure and anisotropy in Ni_3Al single crystals," *Metal Science and Heat Treatment*, vol. 36, no. 2, pp. 99–102, 1994.

[3] A. Chiba and S. Hanada, "Relationship between the APD structure and ductility of rapidly solidified Ni_3Al alloys," *Intermetallics*, vol. 4, no. 1, pp. 55–59, 1996.

[4] P. Jozwik, E. Jezierska, and Z. Bojar, "TEM investigations of Ni_3Al-based intermetallic polycrystals," *Materials Chemistry and Physics*, vol. 81, no. 2-3, pp. 448–451, 2003.

[5] O. Hunziker and W. Kurz, "Solidification microstructure maps in Ni-Al alloys," *Acta Materialia*, vol. 45, no. 12, pp. 4981–4992, 1997.

[6] T. Mawari and T. Hirano, "Effects of unidirectional solidification conditions on the microstructure and tensile properties of Ni_3Al," *Intermetallics*, vol. 3, no. 1, pp. 23–33, 1995.

[7] A. Inoue, H. Tomioka, and T. Masumoto, "An improvement of ductility and strength of the L12 compounds in Ni-Al-X (X = Cr, Mn, Fe, Co or Si) systems by melt quenching," *Journal of Materials Science Letters*, vol. 1, no. 9, pp. 377–380, 1982.

[8] R. Goetzinger, M. Barth, D. M. Herlach, O. Hunziker, and W. Kurz, "Disorder trapping in Ni_3(Al, Ti) by solidification from the undercooled melt," *Materials Science and Engineering: A*, vol. 226–228, pp. 415–419, 1997.

[9] J. Sun, C. S. Lee, and J. K. L. Lai, "Deformation microstructure of Ni_3Al intermetallic compound macroalloyed with Pd," *Materials Letters*, vol. 31, no. 1-2, pp. 1–4, 1997.

[10] B. A. Pint, S. A. Speakman, C. J. Rawn, and Y. Zhang, "Deformation and phase transformations during the cyclic oxidation of Ni-Al and Ni-Pt-Al," *The Journal of the Minerals, Metals & Materials Society*, vol. 58, no. 1, pp. 47–52, 2006.

[11] D. Lee, M. L. Santella, I. M. Anderson, and G. M. Pharr, "Thermal aging effects on the microstructure and short-term oxidation behavior of a cast Ni_3Al alloy," *Intermetallics*, vol. 13, no. 2, pp. 187–196, 2005.

[12] M. Haerig and S. Hofmann, "Mechanisms of Ni_3Al oxidation between 500°C and 700°C," *Applied Surface Science*, vol. 125, no. 1, pp. 99–114, 1998.

[13] U. Bardi, A. Atrei, and G. Rovida, "Initial stages of oxidation of the Ni_3Al alloy: a study by X-ray photoelectron spectroscopy and low energy He+ scattering," *Surface Science*, vol. 239, no. 1-2, pp. L511–L516, 1990.

[14] C. Mei, S. Patu, S. Changxu, and S. Jianian, "Effects of B+ and Cr+ ion implantation on the oxidation of Ni_3Al," *Journal of Materials Science*, vol. 28, no. 20, pp. 5508–5513, 1993.

[15] A. Velon and I. Olefjord, "Oxidation behavior of Ni_3Al and Fe_3Al: II. Early stage of oxide growth," *Oxidation of Metals*, vol. 56, no. 5-6, pp. 425–452, 2001.

[16] T. Norby and P. Kofstad, "Electronic, ionic, and protonic conductivities of a commercial, polycrystalline α-Al_2O_3," *High Temperatures-High Pressures*, vol. 20, pp. 345–360, 1988.

[17] D. B. Lee and M. L. Santella, "High temperature oxidation of Ni_3Al alloy containing Cr, Zr, Mo, and B," *Materials Science and Engineering: A*, vol. 374, no. 1-2, pp. 217–223, 2004.

[18] S. G. Addepalli, B. Ekstrom, N. P. Magtoto, J. Lin, and J. A. Kelber, "STM atomic-scale characterization of the γ'-Al_2O_3 film on Ni_3Al(111)," *Surface Science*, vol. 442, no. 3, pp. 385–389, 1999.

[19] A. M. Venezia and C. M. Loxton, "Low pressure oxidation of Ni_3Al alloys at elevated temperatures as studied by X-ray photoelectron spectroscopy and Auger spectroscopy," *Surface Science*, vol. 194, no. 1-2, pp. 136–148, 1988.

[20] A. M. Venezia, C. M. Loxton, and J. A. Horton, "Temperature and pressure effects for oxygen adsorption and oxidation of Ni_3Al alloyed with chromium and zirconium," *Surface Science*, vol. 225, no. 1-2, pp. 195–205, 1990.

[21] U. Bardi, A. Atrei, and G. Rovida, "Initial stages of oxidation of the Ni_3Al alloy: structure and composition of the aluminum oxide overlayer studied by XPS, LEIS and LEED," *Surface Science*, vol. 268, no. 1–3, pp. 87–97, 1992.

[22] P. Pérez, J. L. González-Carrasco, P. Adeva, V. A. C. Haanappel, and M. F. Stroosnijder, "Effect of Cr- and Y-implantation on oxidation behaviour of powder metallurgical Ni_3Al," *Materials Science and Technology*, vol. 15, no. 3, pp. 345–351, 1999.

[23] M. Garza, N. P. Magtoto, and J. A. Kelber, "Characterization of oxidized Ni_3Al(110) and interaction of the oxide film with water vapor," *Surface Science*, vol. 519, no. 3, pp. 259–268, 2002.

[24] V. A. C. Haanappel, P. Pérez, J. L. González-Carrasco, and M. F. Stroosnijder, "The cyclic oxidation behaviour of PM Ni_3Al in air at elevated temperatures: the effect of Cr- and Y-implantation," *Intermetallics*, vol. 6, no. 5, pp. 347–356, 1998.

[25] T. T. Chang, Y. C. Pan, and T. H. Chuang, "The oxidation behavior of Ni_3Al-Zr alloys with various zirconium contents," *Journal of Alloys and Compounds*, vol. 243, no. 1-2, pp. 126–132, 1996.

[26] D. B. Lee and D. J. Kim, "The oxidation of Ni_3Al containing decomposed SiC-particles," *Intermetallics*, vol. 9, no. 1, pp. 51–56, 2001.

[27] W. W. Lee, D. B. Lee, M. H. Kim, and S. C. Ur, "High temperature oxidation of an oxide-dispersion strengthened NiAl," *Intermetallics*, vol. 7, no. 12, pp. 1361–1366, 1999.

[28] A. Velon and D. Q. Yi, "Influence of Cr on the Oxidation of Fe_3Al and Ni_3Al at 500°C," *Oxidation of Metals*, vol. 57, pp. 13–31, 2002.

[29] V. Deodeshmukh, N. Mu, B. Li, and B. Gleeson, "Hot corrosion and oxidation behavior of a novel Pt+ Hf-modified γ'-$Ni_3Al+\gamma$-Ni-based coating," *Surface and Coatings Technology*, vol. 201, no. 1, pp. 3836–3840, 2006.

[30] F. Qin, J. W. Anderegg, C. J. Jenks, B. Gleeson, D. J. Sordelet, and P. A. Thiel, "The effect of Pt on Ni_3Al surface oxidation at low-pressures," *Surface Science*, vol. 601, no. 1, pp. 146–154, 2007.

[31] S. J. Hong, G. H. Hwang, W. K. Han, and S. G. Kang, "Cyclic oxidation of Pt/Pd-modified aluminide coating on a nickel-based superalloy at 1150°C," *Intermetallics*, vol. 17, no. 6, pp. 381–386, 2009.

[32] B. Gleeson, N. Mu, and S. Hayashi, "Compositional factors affecting the establishment and maintenance of Al_2O_3 scales on Ni-Al-Pt systems," *Journal of Materials Science*, vol. 44, no. 7, pp. 1704–1710, 2009.

[33] A. V. Ruban and H. L. Skriver, "Calculated site substitution in ternary γ'-Ni_3Al: temperature and composition effects," *Physical Review B*, vol. 55, no. 2, pp. 856–874, 1997.

[34] C. Wolverton and D. De Fontaine, "Site substitution of ternary additions to Ni_3Al (γ') from electronic-structure calculations," *Physical Review B*, vol. 49, no. 17, pp. 12351–12354, 1994.

[35] C. Y. Geng, C. Y. Wang, and T. Yu, "Site preference and alloying effect of platinum group metals in γ'-Ni_3Al," *Acta Materialia*, vol. 52, no. 18, pp. 5427–5433, 2004.

[36] C. Jiang and B. Gleeson, "Site preference of transition metal elements in Ni$_3$Al," *Scripta Materialia*, vol. 55, no. 5, pp. 433–436, 2006.

[37] C. Jiang, D. J. Sordelet, and B. Gleeson, "Site preference of ternary alloying elements in Ni$_3$Al: a first-principles study," *Acta Materialia*, vol. 54, no. 4, pp. 1147–1154, 2006.

[38] B. Bhattacharya and R. K. Ray, "Deformation behavior of a Ni$_3$Al (B, Zr) alloy during cold rolling: part I. Changes in order and structure," *Metallurgical and Materials Transactions A*, vol. 31, no. 12, pp. 3001–3010, 2000.

[39] Y. Xu, S. Kameoka, K. Kishida, M. Demura, A. P. Tsai, and T. Hirano, "Catalytic properties of Ni$_3$Al intermetallics for methanol decomposition," *Materials Transactions*, vol. 45, no. 11, pp. 3177–3179, 2004.

[40] L. Lu, M. O. Lai, and S. Zhang, "Evolution and characterization of a Ni$_3$Al intermetallic compound during mechanical alloying," *Materials & Design*, vol. 15, no. 2, pp. 79–86, 1994.

[41] T. Hirano, "Improvement of room temperature ductility of stoichiometric Ni$_3$Al by unidirectional solidification," *Acta metallurgica et materialia*, vol. 38, no. 12, pp. 2667–2671, 1990.

[42] B. D. Cullity and S. R. Stock, *Elements of X-ray Diffraction*, , pp. 125–170, Prentice Hall, Pearson New Iinternational Edition, Upper Saddle River, NJ, USA, 2014.

[43] R. Seymour, A. Hemeryck, K. I. Nomura et al., "Nanoindentation of NiAl and Ni$_3$Al crystals on (100), (110), and (111) surfaces: a molecular dynamics study," *Applied Physics Letters*, vol. 104, no. 14, p. 141904, 2014.

[44] G. F. Cotterill, H. Niehus, and D. J. O'Connor, "An STM study of the initial stages of oxidation of Ni$_3$Al (110)," *Surface Review and Letters*, vol. 3, no. 3, pp. 1355–1363, 1996.

[45] Y. G. Shen, D. J. O'Connor, and R. J. MacDonald, "Studies of surface composition, structure and oxygen adsorption of Ni$_3$Al (110) by Li+ and He+ ion scattering," *Surface and Interface Analysis*, vol. 18, no. 10, pp. 729–739, 1992.

[46] A. Rosenhahn, J. Schneider, C. Becker, and K. Wandelt, "Oxidation of Ni$_3$Al (111) at 600, 800, and 1050 K investigated by scanning tunneling microscopy," *Journal of Vacuum Science & Technology A: Vacuum, Surfaces, and Films*, vol. 18, no. 4, pp. 1923–1927, 2000.

[47] S. Degen, A. Krupski, M. Kralj et al., "Determination of the coincidence lattice of an ultra thin Al$_2$O$_3$ film on Ni$_3$Al (111)," *Surface science*, vol. 576, no. 1–3, pp. L57–L64, 2005.

[48] A. Rosenhahn, J. Schneider, C. Becker, and K. Wandelt, "The formation of Al$_2$O$_3$-layers on Ni$_3$Al (111)," *Applied Surface Science*, vol. 142, no. 1–4, pp. 169–173, 1999.

[49] S. P. Chen, A. F. Voter, and D. J. Srolovitz, "Oscillatory surface relaxations in Ni, Al, and their ordered alloys," *Physical Review Letters*, vol. 57, no. 11, pp. 1308–1311, 1986.

[50] W. J. Chia and Y. W Chung, "Surface spectroscopy and temperature-programmed desorption studies of the interaction of water vapor with Ni$_3$(Al, Ti) (100) and (111) surfaces as a function of temperature," *Intermetallics*, vol. 3, no. 6, pp. 505–509, 1995.

[51] O. Hunziker and W. Kurz, "Directional solidification and phase equilibria in the Ni-Al system," *Metallurgical and Materials Transactions A*, vol. 30, no. 12, pp. 3167–3175, 1999.

[52] G. Rosas, R. Esparza, A. Bedolla, O. Flores, and R. Perez, "Effect of Li alloying on the microstructure and mechanical properties of Ni$_3$Al," *Advances in Technology of Materials and Materials Processing Journal*, vol. 9, pp. 99–102, 2007.

[53] M. H. Jacobs, *TALAT Lecture 1203: Phase Diagrams*, European Aluminium Association, Bruxelles, Belgium, 2010.

[54] E. J. Lavernia and T. S. Srivatsan, "The rapid solidification processing of materials: science, principles, technology, advances, and applications," *Journal of Materials Science*, vol. 45, no. 2, pp. 287–325, 2010.

[55] Z. Jingchen and Y. Ping, *The Effect of Cooling Rate of Solidification on Microstructure and Alloy Element Segregation of as Cast Alloy 718*, pp. 133–140, Central Iron and Steel Research Institute, Beijing, China, 2015.

[56] J. Xu, U. Herr, T. Klassen, and R. S. Averback, "Formation of supersaturated solid solutions in the immiscible Ni-Ag system by mechanical alloying," *Journal of Applied Physics*, vol. 79, no. 8, pp. 3935–3945, 1996.

[57] J. Zhou and J. T. Guo, "Effect of Ag alloying on the microstructure of NiAl," *Materials Letters*, vol. 56, no. 3, pp. 178–182, 2002.

[58] J. Zhou and J. T. Guo, "Effect of Ag alloying on microstructure, mechanical and electrical properties of NiAl intermetallic compound," *Materials Science and Engineering: A*, vol. 339, no. 1-2, pp. 166–174, 2003.

[59] L. Sheng, W. Zhang, J. Guo, F. Yang, Y. Liang, and H. Ye, "Effect of Au addition on the microstructure and mechanical properties of NiAl intermetallic compound," *Intermetallics*, vol. 18, no. 4, pp. 740–744, 2010.

[60] C. Meng, J. Guo, and Z. Hu, "Mechanism of macroalloying-induced ductility in Ni$_3$Al," *Journal of Materials Science & Technology*, vol. 10, pp. 279–284, 1994.

[61] M. J. Li, X. F. Sun, H. R. Guan, X. X. Jiang, and Z. Q. Hu, "The degradation of (Ni,Pd)Al coatings on superalloy IN738 during isothermal oxidation," *Surface and Coatings Technology*, vol. 185, no. 2-3, pp. 172–177, 2004.

[62] M. J. Li, X. F. Sun, H. R. Guan, X. X. Jiang, and Z. Q. Hu, "Cyclic oxidation behavior of palladium-modified aluminide coating," *Surface and Coatings Technology*, vol. 167, no. 1, pp. 106–111, 2003.

[63] D. Oquab and D. Monceau, "In-situ SEM study of cavity growth during high temperature oxidation of β-(Ni,Pd)Al," *Scripta Materialia*, vol. 44, no. 12, pp. 2741–2746, 2001.

[64] Y. Zhang, J. A. Haynes, W. Y. Lee et al., "Effects of Pt incorporation on the isothermal oxidation behavior of chemical vapor deposition aluminide coatings," *Metallurgical and Materials Transactions A*, vol. 32, no. 7, pp. 1727–1741, 2001.

[65] P. Peréz, M. Eddahbi, J. L. González-Carrasco, and P. Adeva, "Effect of the processing route on the oxidation behaviour of a Ni$_3$Al powder metallurgy alloy," *Intermetallics*, vol. 7, no. 6, pp. 679–687, 1999.

[66] J. J. Ramos-Hernandez, J. Porcayo-Calderon, V. M. Salinas-Bravo, C. D. Arrieta-Gonzalez, J. G. Gonzalez-Rodriguez, and L. Martinez-Gomez, "Phase stability diagrams for high temperature corrosion processes," *Mathematical Problems in Engineering*, vol. 2013, pp. 1–7, 2013.

[67] A. Atkinson, R. I. Taylor, and A. E. Hughes, "A quantitative demonstration of the grain boundary diffusion mechanism for the oxidation of metals," *Philosophical Magazine A*, vol. 45, no. 5, pp. 823–833, 1982.

[68] D. Naumenko, B. Gleeson, E. Wessel, L. Singheiser, and W. J. Quadakkers, "Correlation between the microstructure, growth mechanism, and growth kinetics of alumina scales on a FeCrAlY alloy," *Metallurgical and Materials Transactions A*, vol. 38, no. 12, pp. 2974–2983, 2007.

[69] W. J. Quadakkers, D. Naumenko, E. Wessel, V. Kochubey, and L. Singheiser, "Growth rates of alumina scales on Fe–Cr–Al alloys," *Oxidation of Metals*, vol. 61, no. 1-2, pp. 17–37, 2004.

[70] Y. Cadoret, D. Monceau, M. Bacos, P. Josso, V. Maurice, and P. Marcus, "Effect of platinum on the growth rate of the oxide scale formed on cast nickel aluminide intermetallic alloys," *Oxidation of Metals*, vol. 64, no. 3-4, pp. 185–205, 2005.

[71] S. Hayashi and B. Gleeson, "Early-stage oxidation behavior of Pt-modified γ'-Ni_3Al-based alloys with and without Hf addition," *Oxidation of Metals*, vol. 71, no. 1-2, pp. 5–19, 2009.

[72] M. W. Brumm and H. J Grabke, "The oxidation behaviour of NiAl-I. Phase transformations in the alumina scale during oxidation of NiAl and NiAl-Cr alloys," *Corrosion Science*, vol. 33, no. 11, pp. 1677–1690, 1992.

[73] S. C. Choi, H. J. Cho, Y. J. Kim, and D. B. Lee, "High-temperature oxidation behavior of pure Ni_3Al," *Oxidation of Metals*, vol. 46, no. 1-2, pp. 51–72, 1996.

[74] J. D. Kuenzly and D. L. Douglass, "The oxidation mechanism of Ni_3Al containing Yttrium," *Oxidation of Metals*, vol. 8, no. 3, pp. 139–178, 1974.

[75] S. Ochiai, T. Suzuki, Y. Kojima, M. Kobayashi, and Y. Torisaka, "Effect of yttrium addition on the high-temperature oxidation resistance of Ni_3Al alloy," *Journal of the Japan Institute of Metals and Materials*, vol. 53, no. 6, pp. 585–592, 1989.

[76] N. Birks, G. H. Meier, and F. S. Pettit, "High-temperature corrosion resistance," *Journal of the Minerals, Metals & Materials Society*, vol. 39, no. 12, pp. 28–31, 1987.

[77] G. Cao, L. Geng, Z. Zheng, and M. Naka, "The oxidation of nanocrystalline Ni_3Al fabricated by mechanical alloying and spark plasma sintering," *Intermetallics*, vol. 15, no. 12, pp. 1672–1677, 2007.

[78] N. Mu, T. Izumi, L. Zhang, and B. Gleeson, "The development and performance of novel Pt+Hf-modified γ'-Ni_3Al +γ-Ni bond coatings for advanced thermal barrier coatings systems," in *Superalloys 2008*, R. C. Reed, K. A. Green, P. Caron et al, Eds., TMS (The Minerals, Metals & Materials Society), 2008.

[79] C. Jiang and B. Gleeson, "Surface segregation of Pt in γ'-Ni_3Al: a first-principles study," *Acta Materialia*, vol. 55, no. 5, pp. 1641–1647, 2007.

[80] Y. Niu, X. J. Zhang, Y. Wu, and F. Gesmundo, "The third-element effect in the oxidation of Ni–xCr–7Al (x=0, 5, 10, 15at.%) alloys in 1atm O_2 at 900–1000°C," *Corrosion Science*, vol. 48, no. 12, pp. 4020–4036, 2006.

[81] J. Porcayo-Calderon, O. Sotelo-Mazon, V. M. Salinas-Bravo, C. D. Arrieta-Gonzalez, J. J. Ramos-Hernandez, and C. Cuevas-Arteaga, "Electrochemical performance of Ni_20Cr coatings applied by combustion powder spray in $ZnCl_2$-KCl molten salts," *International Journal of Electrochemical Science*, vol. 7, pp. 1134–1148, 2012.

[82] A. Luna-Ramirez, J. Porcayo-Calderon, G. Salinas-Solano, C. D. Arrieta-Gonzalez, V. M. Salinas-Bravo, and L. Martinez, "Electrochemical performance of Fe-Al intermetallic alloys with addition of Li, Ni and Ce in $NaVO_3$ at 700°C," *International Journal of Electrochemical Science*, vol. 8, pp. 4641–4653, 2013.

[83] J. Porcayo-Calderon, O. Sotelo-Mazon, M. Casales-Diaz, J. A. Ascencio-Gutierrez, V. M. Salinas-Bravo, and L. Martinez-Gomez, "Electrochemical study of Ni_20Cr coatings applied by HVOF process in $ZnCl_2$-KCl at high temperatures," *Journal of Analytical Methods in Chemistry*, vol. 2014, pp. 1–11, 2014.

[84] G. Salinas-Solano, J. Porcayo-Calderon, J. G. Gonzalez-Rodriguez, V. M. Salinas-Bravo, J. A. Ascencio-Gutierrez, and L. Martinez-Gomez, "High temperature corrosion of inconel 600 in NaCl-KCl molten salts," *Advances in Materials Science and Engineering*, vol. 2014, pp. 1–9, 2014.

[85] O. Sotelo-Mazon, J. Porcayo-Calderon, C. Cuevas-Arteaga et al., "Corrosion performance of Ni-based alloys in sodium metavanadate," *International Journal of Electrochemical Science*, vol. 11, pp. 1868–1882, 2016.

[86] J. Doychak, J. L. Smialek, and C. A. Barrett, "The oxidation of Ni-rich Ni-Al intermetallics," in *Oxidation of High Temperature Intermetallics*, T. Grobstein and J. Doychak, Eds., p. 41, Minerals, Metals & Material Society, 1988.

[87] K. Zhao, Y. B. Zhou, Y. H. Ma, L. H. Lou, and Z. Q. Hu, "Effect of microstructure on the oxidation behavior of two nickel-based superalloys," *Corrosion*, vol. 61, no. 10, pp. 961–967, 2005.

[88] G. Liu, M. Li, M. Zhu, and Y. Zhou, "Transient of alumina oxide scale on β-NiAl coated on M38G alloy at 950°C," *Intermetallics*, vol. 15, no. 10, pp. 1285–1290, 2007.